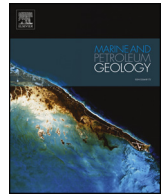




ELSEVIER

Contents lists available at ScienceDirect

Marine and Petroleum Geology

journal homepage: www.elsevier.com/locate/marpetgeo

Research paper

Characterization of lacustrine mixed fine-grained sedimentary rocks using coupled chemostratigraphic-petrographic analysis: A case study from a tight oil reservoir in the Jimusar Sag, Junggar Basin

Shaomin Zhang^{a,*}, Yingchang Cao^{a,b,**}, Keyu Liu^{a,b}, Jens Jahren^c, Kelai Xi^a, Rukai Zhu^d, Tian Yang^a, Xu Cao^e, Wei Wang^a

^a School of Geosciences, China University of Petroleum (East China), Qingdao, Shandong, 266580, China

^b Laboratory for Marine Mineral Resources, Qingdao National Laboratory for Marine Science and Technology, Qingdao, 266071, China

^c Department of Geosciences, University of Oslo, P.O. Box 1047, Blindern, 0316, Oslo, Norway

^d Research Institute of Petroleum Exploration & Development, Beijing, 100083, China

^e Department of Earth Science, Durham University, Durham, DH1 3LE, UK

ARTICLE INFO

Keywords:

Mixed sedimentary rocks
Lithologies
Chemostratigraphy
Trace and major elements
Deposition environmental settings
Jimusar sag

ABSTRACT

Mixed deposits are sediments consisting of external clastic (epiclastic or terrigenous), intrabasinal components and pyroclastic components. The mixture, comprising variable amounts of the three components, is defined as “mixed sedimentary rocks”. The Permian Lucaogou Formation (P₂l) in the Jimusar Sag of the Junggar Basin is a promising tight oil target in western China, the fine-grained mixed sedimentary rocks of which are rich in organic matter (OM) and two sweet spot intervals with relatively high porosity. However, the sediment composition, provenance and deposition environmental settings have not been studied in detail. In this study coupled chemostratigraphic-petrographic analysis were used to reconstruct their depositional environments. The results show that the fine-grained sedimentary rocks have three major sediment sources, external clastic input (terrigenous clastics), intrabasinal autochthonous to parautochthonous (carbonates, siliceous skeletal debris and OM) and pyroclastic input. Main lithofacies include siltstone/fine sandstone, mudstone, dolomite and tuffite. The silt/sandstones were mainly sourced from rocks with calc-alkaline composition, while the tuffaceous sedimentary rocks were sourced from high-K calc-alkaline rocks. Elemental proxies suggest that the carbonate rocks were generally deposited under warm and arid conditions, whereas the fine-grained clastic sediments were deposited under relatively humid conditions. The muddy or silty tuffaceous mixed rocks were deposited under relatively reducing conditions compared with carbonates and sandstones. Variations of lithofacies and OM accumulation of different intervals reflect changing deposition environmental settings, and the frequently altered high TOC content rocks and good reservoirs are benefit for tight oil formation. The work may provide some useful insights and serve as a reference for studying other mixed fine-grained sedimentary rocks and tight oil plays in similar lacustrine basins elsewhere.

1. Introduction

With increasing demand for oil and gas resources and declining of the conventional oil and gas reserve, tight petroleum reservoirs have become new unconventional petroleum plays (Jarvie et al., 2007; Jia et al., 2012; Xi et al., 2016). Tight oil reservoirs in China, which are mostly developed in lacustrine sedimentary sequences, mainly include tight carbonates, tight sandstones/siltstones and mudstones, with reservoirs being commonly hosted in mixed sedimentary rocks (Jia et al.,

2012; Zou et al., 2012a, 2012b). These mixed sedimentary rocks, most of which are fine-grained, are typical tight oil reservoirs (Ma et al., 2016a; Zou et al., 2015). However, reports on mixed fine-grained rocks are still relatively uncommon, and most recent researches mainly focus on mixed siliciclastic-carbonate systems and their depositional environments (Thrana and Talbot, 2006; McNeill et al., 2012; Harper et al., 2015; Chiarella et al., 2017). Mixed fine-grained rocks and associated hydrocarbon plays are quite complicated, as sources-reservoirs-seals are mingled together and controlled primarily by

* Corresponding author.

** Corresponding author. School of Geosciences, China University of Petroleum (East China), Qingdao, Shandong, 266580, China.

E-mail addresses: Zhangshaomin0813@126.com (S. Zhang), cyc8391680@163.com (Y. Cao).

<https://doi.org/10.1016/j.marpetgeo.2018.10.039>

Received 2 July 2018; Received in revised form 15 October 2018; Accepted 22 October 2018

Available online 23 October 2018

0264-8172/ © 2018 Elsevier Ltd. All rights reserved.

sedimentary heterogeneities (Chiarella et al., 2017). The lithologies and depositional characters of mixed fine-grained rocks are controlled by a series of factors, including sediment supply, paleo-climate and paleo-redox and -salinity conditions (Nesbitt and Young, 1982; Liu et al., 2018; Zhang et al., 2018a).

The fine-grained, composition-complicated, frequently stacked nature of rocks results in alternating compositions, structures and textures. This makes it difficult to recognize sediment variations directly from the drilled cores by visual inspection and/or optical microscopy. The lithofacies variability and organic content together with generally dark sediment coloration further increase the difficulty to study these mixed fine-grained deposits. However, the variations in chemical compositions such as major and trace elements are useful for delineating mineralogy, material sources and depositional environments (Nesbitt and Young, 1982; Hayashi et al., 1997; Rowe et al., 2012; Zhou et al., 2015), also help to distinguish reservoir and source rocks.

The middle Permian Lucaogou Formation (P_2l) in the Jimusar Sag, Junggar Basin is a fine-grained mixed sedimentary sequence, composed predominately of carbonates, terrigenous siliciclastic and volcanic materials (Xi et al., 2015; Ma et al., 2017). The P_2l Formation has long been recognized as the most important source rock for the overlying units in the southeastern part of the basin (Fang et al., 2007), as the P_2l Formation is rich in oil-prone organic matter (TOC = 0.03–19.77 wt%, mainly Type I and II kerogen), having reached a favorable thermomaturity level for oil generation with a moderate maturity ($R_o = 0.6$ – 1.0%) (data were collected from Xinjiang Oilfield) (Wu et al., 2017). Recently, the P_2l Formation has received attention as a potential tight oil play in western China (Kuang et al., 2012; Xi et al., 2015; Yang et al., 2015). The P_2l rocks are characterized by strong heterogeneous compositional variations, with thin interbedded layers and rapidly alternating textures, which pose huge challenges in characterizing lithofacies and geochemistry features systematically. The primary aim of this study is to analyze mineralogical and lithological features and deposition environmental settings of mixed fine-grained sedimentary sequence of the P_2l Formation utilizing mineral and elemental data. An in-depth study of these frequently mixed sedimentary rocks and their depositional variability will help better understanding the controlling factors of lacustrine fine-grained mixed sediments, organic matter accumulations and hydrocarbon exploration potential and favorable targets.

2. Geologic and depositional setting

The Junggar Basin in the northern part of the Xinjiang Uygur Autonomous Region, western China is a typical intracontinental superimposed basin, evolving from a Paleozoic foreland basin, through a Mesozoic fault-depression basin to a Cenozoic foreland basin (Fang et al., 2007; Cao et al., 2016; Wu et al., 2016). The Jimusar Sag is located in the southeastern part of the Junggar Basin (Fig. 1a and b) and covers an area of approximately 1300 km². The sag is bound by the Jimusar fault to the north, the Santai fault to the south, the Xidi fault and the Laozhuangwan fault to the west, and pinching out to the eastern Guxi uplift (Fig. 1c). The Jimusar Sag has experienced multi-stages of tectonic subsidence and uplift, which are thought to have controlled the basin evolution and structural configuration. It is a half-graben sag with faulting in the west and overlapping on the Carboniferous basement in the east. The sag is covered by sedimentary rocks from the Permian to Quaternary period (Fig. 1d). The Jimusar Sag was gradually subsided during the Hercynian tectonic episode (late Carboniferous – Permian period), with contemporaneous rifting and volcanic activities around the Junggar Basin (Luo et al., 2007; Mao et al., 2012), forming Jingjingzigou (P_2j), Lucaogou (P_2l) and Wutonggou (P_3wt) formations. Mudstones interbedded with sandstones/siltstones, carbonates and tuffaceous rocks deposited during the P_2l time, serve as major source rocks in the Jimusar Sag. From the Indosinian period to the middle Yanshan tectonic episodes (Triassic – Jurassic), the sag was

under warm and humid climate (Wu et al., 2016), and the Jiucaiyuan (T_{1j}), Shaofanggou (T_{1s}) and Kelamayi (T_{2k}) formations, and the Badaowan (J_{1b}), Sangonghe (J_{1s}), Xishanyao (J_{2x}), Toutunhe (J_{2t}) and Qigu (J_{3q}) formations were deposited (Fig. 2a). There was intensive erosion in the later Jurassic due to the uplift of the Qitai uplift. The sag was subsequently strongly deformed during the Late Yanshan Orogeny and was finally developed after the Himalayan movement (Cai et al., 2000), during which the Jurassic and Cretaceous strata were eroded and the Paleogene strata directly overlay on them with angular unconformity (Fig. 1d).

The Lucaogou Formation (P_2l) was deposited under saline lacustrine conditions during the mid-Permian (Ma et al., 2017). The formation is characterized by fine-grained mixed sedimentary sequences containing layers of mudstones interbedded with carbonates, siltstone/fine sandstone and pyroclastics (Xi et al., 2015; Zhang et al., 2018b). The P_2l Formation is found across the entire sag and has a large thickness of 200–350 m. It can be divided into lower (P_{2l_1}) and upper (P_{2l_2}) sections based on an internal maximum flooding surface (Fig. 2b) (Kuang et al., 2013).

3. Data and methods

3.1. Samples and tests

Some of the data presented here are provided by the Xinjiang Oilfield Company, PetroChina, including wireline logging data from 15 wells within the P_2l Formation, X-ray diffraction (XRD) data of 188 rock samples, and 299 total organic carbon (TOC) contents and Rock-Eval pyrolysis results.

A total of 500 m cores of the P_2l Formation from 15 wells in the Jimusar Sag were logged for the purpose of evaluating the source rocks and depositional characteristics. Over 350 samples were collected from these drill cores and used for various measurements and analyses. A total of 250 blue epoxy resin impregnated thin sections were examined under a polarizing Zeiss microscope (Axio Scope A1) for grain size, rock composition and texture analyses. Based on the results, 25 representative gold-coated samples were further selected and analyzed using a JEOL LSM-6460LV scanning electron microscopy (SEM) (15 kv acceleration voltage, 10 nA beam current). The SEM was equipped with an energy dispersive X-ray spectrometer (EDS) for semi-quantitative mineral identification by spot chemical analyses and also coupled with backscattered electron (BSE) imaging system.

A total of 32 rock samples were prepared for bulk XRD analyses to complement optical petrography and quantify mixed rocks constituents. About 3.0 g of each sample was milled in a McCrone micronizing mill and dried to get random powder. The powder diffraction patterns were obtained using D/max-Ultima IV-ray diffractometer with Cu K α radiation, 40 kV pipe pressure, 40 mA conduit flow and 2° 2 θ /min scanning speed.

3.2. Elements detected

Element measurements were undertaken systematically on clean core cut surfaces from wells J-174, J-30, J-251, J-32, J-301, J-302 and J-303 within the P_2l Formation in the Jimusar Sag using Niton XL3t GOLDD+ handheld energy dispersive portable X-ray spectrometers (pXRF). The pXRF instrument was carefully and directly laid onto slabbed clean surfaces of the drilled cores with the beam (area diameter less than 1 cm) pointing downward. We utilized the “Mining mode” protocol to determine the major element oxides (SiO₂, Al₂O₃, Fe₂O₃, K₂O, CaO, MgO and P₂O₅) undertaken with a duration time of 120 s and the “Soil mode” protocol to determine the trace elements (Mo, Zr, Sr, U, Rb, Th, Pb, Au, As, Hg, Li, Be, Sc, Se, V, Ni, Cr, Co, Mn, Ti, Cu, Zn, W, Ag, Pd, Cd, Sb, Cs, Te, Sn, Ba, Bi, Nb, Cl) concentrations using a counting time of 60 s. The concentrations of the elements and oxides were expressed in ppm. The relative standard deviation (RSD) ranges

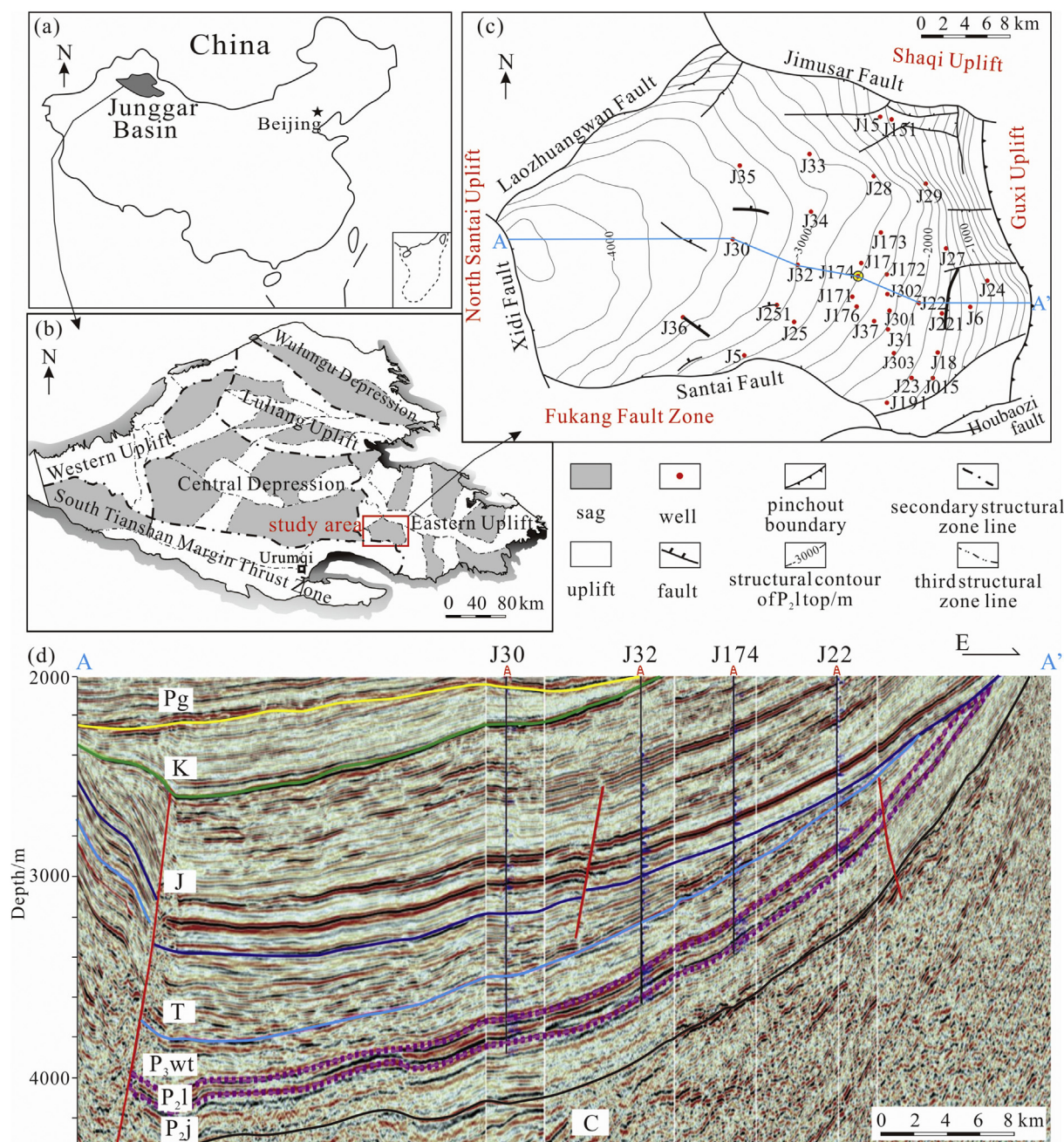


Fig. 1. Location of the study area; (a) Location of the Junggar Basin in western China; (b) The primary sags and uplifts in the Junggar Basin and location of the Jimusar Sag; (c) Structure contour of top of the Lucaogou formation, location of major wells and structural configuration of the Jimusar Sag; (d) Seismic section showing the stratigraphic framework of the Jimusar Sag, and the location of the seismic section is shown by line AA' in (c). Pg-Paleogene, K-Cretaceous, J-Jurassic, T-Triassic, P_{3wt}-upper Permian Wutonggou Formation, P_{2l}-middle Permian Lucaogou Formation, P_{2j}-middle Permian Jingjingzigou Formation.

from 0.21% (Fe) to 8.2% (Cd), within the RSD criteria of 10% for definitive data quality. Some 2020 data points on 445 m cores from the above wells were collected with both the “Soil” and “Mining” modes, respectively.

A total of 16 fine-grained rock samples of diverse lithologies from the Lucaogou Formation in the study area were selected to measure their bulk and trace elemental geochemistry using X-ray fluorescence spectroscopy (XRF) and then compared with the corresponding results from pXRF. All these rocks were taken from clean drilled cores and powdered into 200-mesh by a pulverizer, then analyzed by XRF in the Analytical Laboratory of Beijing Research Institute of Uranium Geology (BRIUG). Major element concentrations were measured using a melting method of a fused disk, which was prepared in crucibles (made of 95%

Pt-5% Au) with 0.7 g sample, 5.9 g Flux (Lithium tetraborate-fluoride and ammonium nitrate mix) and 1 mL LiBr, then melted under 1150 °C–1250 °C, following the method of Robinson (2003). The sample was then analyzed by an Axios mAX wavelength dispersive X-ray fluorescence spectrometer (WD-XRF) and expressed as weight percent of element oxides (SiO₂, Al₂O₃, Fe₂O₃, TiO₂, MnO, Na₂O, K₂O, CaO, MgO and P₂O₅). The analytical uncertainty was less than 5% for major oxides. Trace elements were measured using a NexION300D Inductively Coupled Plasma source Mass Spectrometer (ICP-MS) with a dissolving method (Liang et al., 2000). About 50 mg of powdered sample was digested with 1 ml HF and 0.5 ml HNO₃ in a sealed PTFE bomb and then put into an oven at about 190 °C for 24 h. After cooling, the bomb was heated to evaporate on a hot plate. Then 0.5 ml HNO₃ were added and

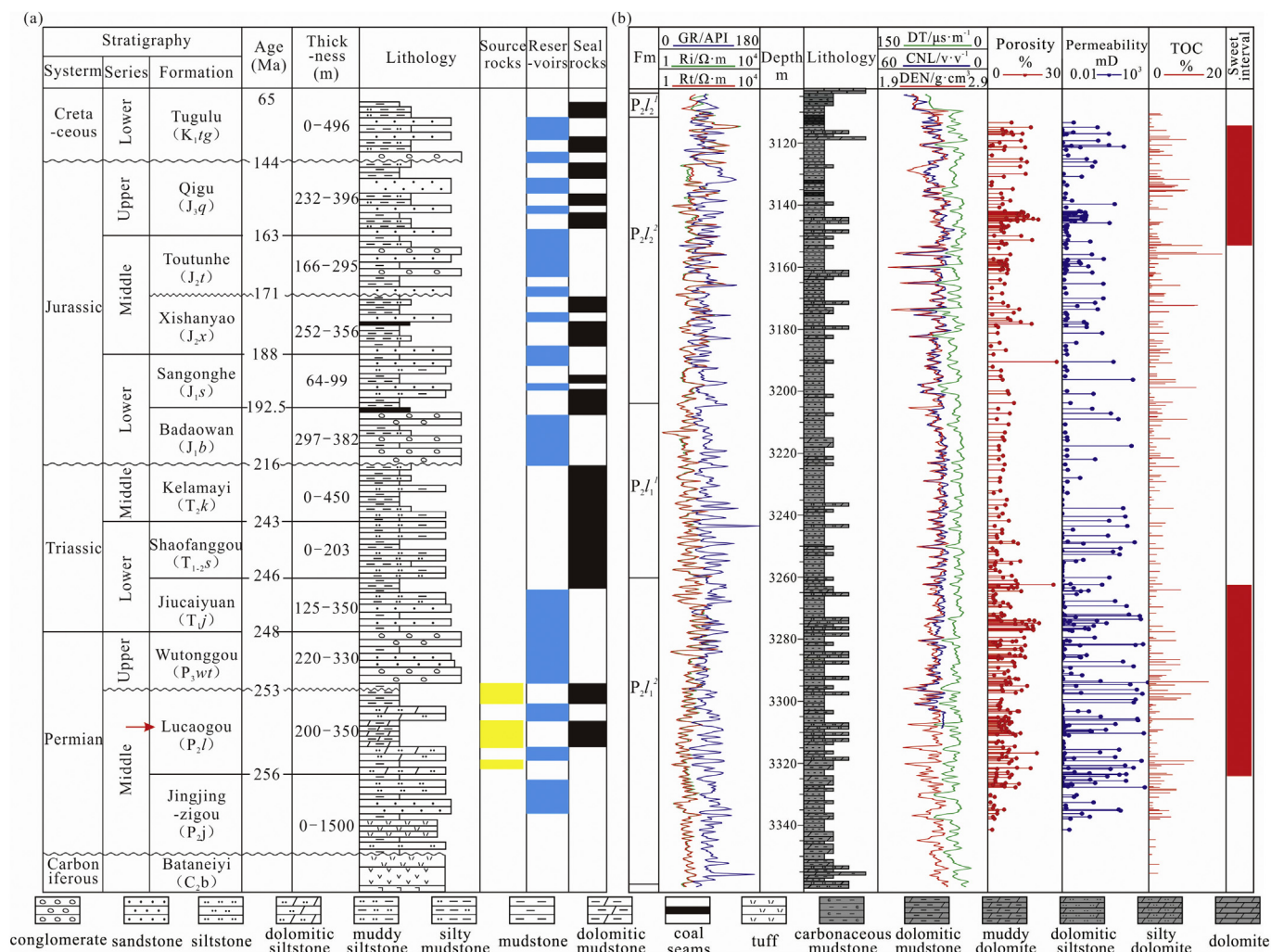


Fig. 2. (a) Generalized stratigraphy of the Jimusar Sag, showing major hydrocarbon combinations (modified from Wu et al., 2016). (b) Composite logging, TOC, porosity and permeability, and sweet spot interval distribution of Well J-174. The location of Well J-174 is shown in Fig.1c.

evaporated the solution in the bomb to dry. After that, 5 ml HNO₃ was again added to the bomb, then sealed and placed into an oven heated to 130 °C for 3 h to dissolve the residues. The final cooling dilution was measured by ICP-MS for trace elements. The results were expressed in ppm (Li, Be, Sc, V, Ni, Cr, Co, Cu, Zn, Ga, Rb, Sr, Zr, Mo, Cd, In, Sb, Cs, Ba, Pb, Th, U, Bi, Nb, and Rare Earth Elements (REE)) with analytical precision being better than 5–10% in relative term.

3.3. Calibrations of powders samples and rock surfaces

Taking the 16 WD-XRF powdered sample measurements as references, different elements from cores measured using the hand-held pXRF were plotted (Fig. 3). The correlations between the two measuring methods were correlated by best fit trend lines (Fig. 3) to correct the concentration data obtained from the pXRF instrument. The pXRF data obtained from cores were then corrected via these best fit calibration curves before their final use in the geochemical analyses (Ryan et al., 2017).

3.4. Statistical analyses

Univariate analyses and R-cluster analyses were performed on the element data using the IBM SPSS Statistics 18 program. Based on the Pearson correlation coefficient, R-mode hierarchical cluster analysis was applied to partition the major and trace elements data into a

number of meaningful multivariate homogeneous groups, in order to investigate the relationship between the elements (Xie et al., 2018) and to refine our understanding of elemental affinities by statistical analyses.

4. Results

4.1. Lithology of mixed sedimentary rocks

4.1.1. Mineral composition

From thin section and XRD analyses, the mineral components of the P₂l Formation are mainly feldspar, quartz and carbonate minerals, with minor amounts of clay minerals, pyrite and analcite. The vertical mineral distribution profile shown in Fig. 4 was established by XRD results of 235 core samples in Well J-174 throughout the P₂l Formation, showing high mineral variabilities as a function of depth. Feldspar, which is the most common mineral component among all, is dominated by plagioclase, ranging from 0% to 73.5% of the bulk mineralogy with an average value of 24.6%, with minor K-feldspar, ranging between 0% and 5% with an average amount of 4.0%. This is followed by quartz, ranging from 4.6% to 52% (average 20.81%). Carbonate minerals contents vary greatly. Dolomite content ranges from trace amounts to 91.5% with an average of 26.56%, whereas calcite ranges from 0 to 84.4%, with most samples containing 0%–20% range averaging 10.3%. Clay mineral contents in the study interval are generally low, primarily

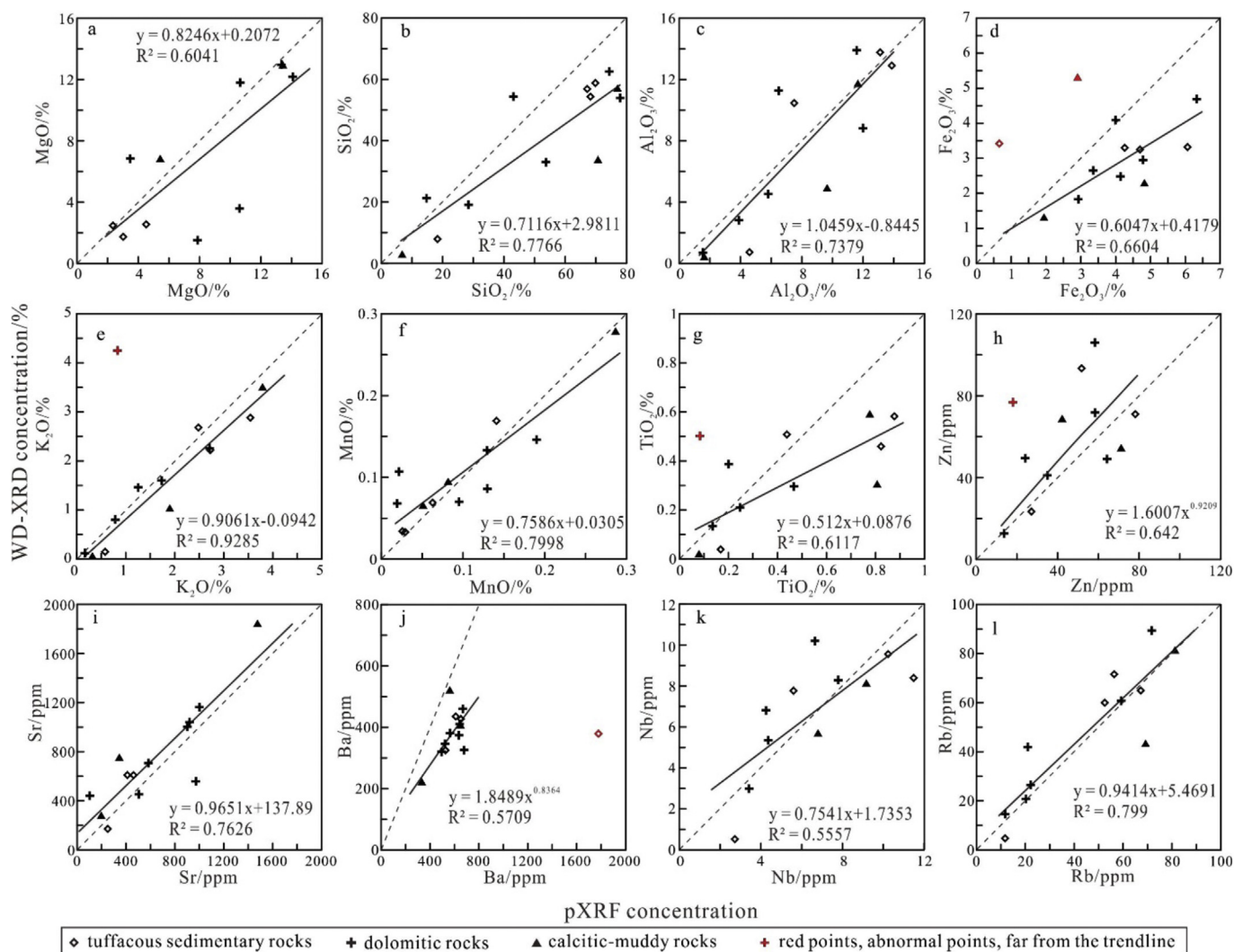


Fig. 3. Scatter plots of calibration measured by pXRF (x-axis) and WD-XRF (y-axis). The units of concentrations for the elements by pXRF are in ppm, the percentage of major oxides (a–g) are calculated from concentrations. The major oxide values (a–g) by WD-XRF are in weight %, while trace elements (h–l) by ICP-MS are in ppm. Dashed lines have a gradient of 1.

in the range of 0%–15% with an average of 11.9%. Clay minerals are dominated by smectite and mixed-layer chlorite-smectite (C/S), with moderate amounts of mixed-layer illite-smectite (I/S) and minor illite and chlorite.

4.1.2. Source components

Three different sediment types are found in the P₂l Formation, with detrital siliciclastic dominated source material, carbonate dominated source material and volcanic dominated source material. The deposition of the formation is a result of a combined effect of lake level fluctuations, provenance and depositional environment (Ma et al., 2017).

Core observations, thin section and SEM analyses indicate that the fine-grained sedimentary rocks in the study area were sourced from three material types, external clastic input (terrigenous clastics), autochthonous to parautochthonous components (carbonates, siliceous skeletal debris and OM) and pyroclastic components.

External clastic components within the P₂l Formation fine-grained rocks consist mainly of quartz, albite, clay minerals and K-feldspar (Fig. 5). Most terrigenous grains are moderately texturally mature, with mainly subangular to subrounded shapes and point-to-line contacts or dispersive distribution. The size of detrital quartz grains ranges from 5 to 100 μm , while the grain sizes of feldspar ranging from 5 to 200 μm

with most grains less than 100 μm . Clay minerals are dominated by smectite and mixed-layer I/S and C/S.

Intrabasinal (autochthonous to parautochthonous) components in the study area include intraclast (e.g. carbonate or siliceous fossil debris, fecal pellets and ooids), carbonate precipitation and organic matter (Pommer and Milliken, 2015) (Fig. 5). Ostracods and some other fossil fragments are replaced by silica and carbonate, generally 25–500 μm in dimensions. Fecal pellets and ooids are abundant in the P₂l Formation, usually sub-rounded to round in shapes and 50–200 μm in diameters. Organic matter, including algae, bacteria and some other bioclastic, as well as solid bitumen, are present in the P₂l Formation fine-grained rocks. The size of the OM fragments varies widely, from 200 μm to 5 cm in dimensions (Fig. 5).

The alkaline pyroclastic components are widespread in the P₂l Formation, including feldspar and quartz pyroclasts and vitroclastics, consists mainly of fine particles, such as silty tuff (0.1–0.01 mm) and fine volcanic dust (< 0.0625 mm) (Fig. 5).

4.1.3. Lithofacies of mixed sedimentary rocks

Optical microscopic and SEM observations with EDS analyses indicate that the mixed sedimentary rocks studied are different from common siliciclastic-calcite series described in the literature (e.g., Harper et al., 2015; McNeill et al., 2004; Mount, 1984). To classify the

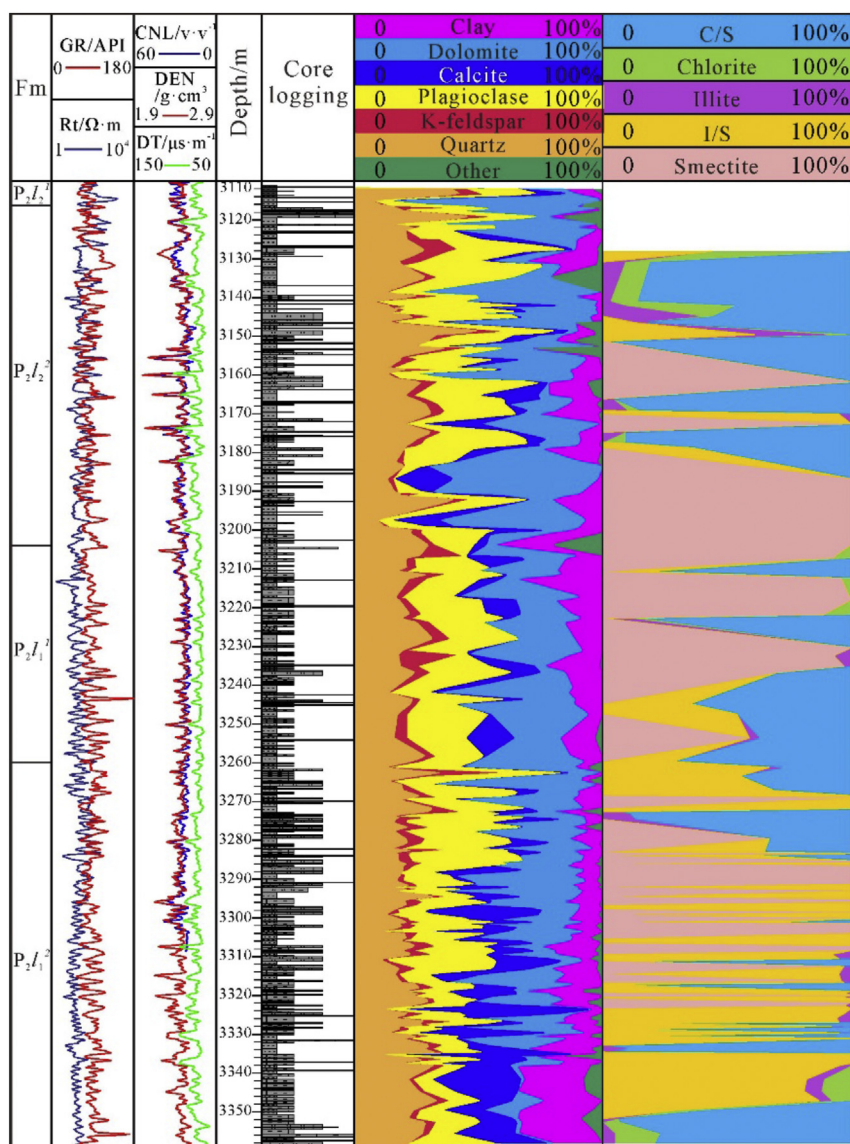


Fig. 4. Mineral compositions and vertical distribution within the P_2l Formation in Well J-174 (Data provided by the Xinjiang Oilfield Company, PetroChina).

lacustrine fine-grained mixed rocks, the three-end member method of rock compositions is used. Terrigenous clastic content, carbonate content and volcanic clastic content are set as the three end members. The main lithofacies are siltstone/fine sandstone, mudstone, dolomite and tuffite, and these lithofacies are further subdivided into 12 lithofacies according to the relative contents of the components.

Fine sandstone/siltstones are widespread across the entire study area, and are characterized predominantly by light gray to gray in color and occurring in massive beds. The beds are sometimes deformed. XRD data shows that this lithofacies is dominated by albite, K-feldspar and quartz, with minor amounts of other minerals, such as clay minerals and pyrite (Fig. 5a, b and c). When the content of micritic dolomite accounts for about 10–50%, dolomitic siltstone is present; when the feldspar and quartz content from pyroclastics take up 10–50% of the whole rock, the rock becomes a tuffaceous fine sandstone/siltstone (Fig. 5d–g). The grains found in the fine sandstone/siltstone are mainly of siliciclastic, volcanic or carbonate intraclasts that comprise moderately to well sorted and subangular to subrounded grains. This lithofacies is typical of near-shore deposits, with the interbedded fine sandstones showing trough cross-bedding while the siltstones showing current and ripple cross-bedding and massive beds.

The mudstone lithofacies is quite common in the P_2l Formation, and

it is quite hard and dark gray to black in color (Fig. 5h). The mudstones lithofacies can be divided into dolomitic mudstone, silty mudstone and tuffaceous mudstone. Dolomitic mudstone is composed of microcrystal dolomite, fine-grained feldspar and quartz and clay minerals. The silty and tuffaceous mudstone are identified from XRD to be composed primarily of siliciclastic components, mainly albite, K-feldspar, and less amounts of quartz, clay minerals (less than 15%) and pyrite (Fig. 5i and j). The tuffaceous matrix is even finer than silt, composed mostly of vitric and crystalline pyroclasts. The mudstone lithofacies are mostly laminated (Fig. 5k, l, m), including four lamina types, rich in dolomite, pyroclastics, siliciclastics or organic matters, respectively. Within these different rock types, the micro-laminae quite commonly show sharp interfaces (Fig. 5m), but the interfaces between pyroclastic and siliciclastic lamina are sometimes gradual. The mudstone lithofacies is generally rich in OM, along with the characteristics of dark color, fine grain size and laminated organic matter. With these features, the mudstone are interpreted to deposit under deep to semi-deep lacustrine conditions (Yang et al., 2017).

Dolomite is the most widely distributed lithofacies in the study area, which include grain dolostone/packstone, dolomicrite and silty or tuffaceous dolomicrite/grain dolostone. In this lithofacies, dolomite is the dominant mineral with a content greater than 50%, while less calcite,

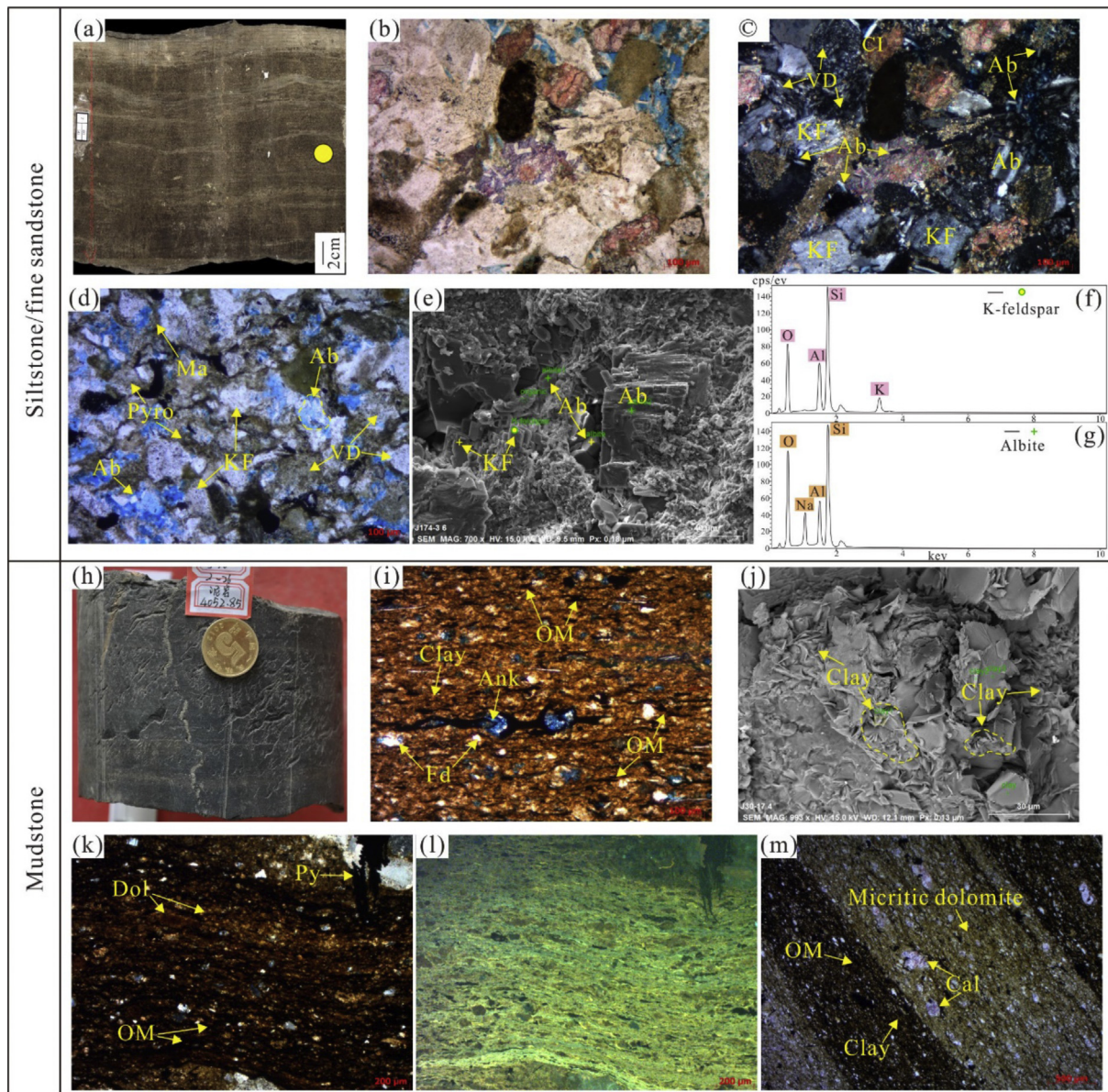


Fig. 5. Core photos and photomicrographs of fine sandstone/siltstone and mudstone lithofacies. (a, b and c) Massive fine sandstone mainly composed of albite, K-feldspar and volcanic detritus (J-174, 3142.2 m). (d–g) Tuffaceous siltstone with increasing volcanic detritus and pyroclastics. (f and g) EDS of the K-feldspar and albite in (e) (J-174, 3125.25 m). (h–j) Mudstone sample, rich in organic matters and clay minerals (J-30, 4052.85 m). (k–l) Laminated mudstone rich in dolomite and organic matter lamina, as well as pyrite. (m) Laminated mudstone with sharply contacted dolomite lamina and clay and OM-rich lamina (J-174, 3319.3 m). VD–volcanic detritus, CI–carbonate intraclast, Kf–K-feldspar, Ab–albite, Ma–matrix, Cal–calcite, Q–quartz, Pyro–pyroclast, Dol–dolomite, Ank–ankerite, OM–organic matter, Py–pyrite.

albite, K-feldspar, quartz, pyrite and minor amount of clay minerals making up the rest of this lithofacies. Grain dolostone/packstone are characterized by whitish to light gray colors (Fig. 6a), and have high content of intraclast, ooids or pellets (generally > 70%) and relatively low terrigenous feldspar content (< 20%). The intraclast grains, pellets and ooids are moderately to well sorted and subrounded to rounded, ranging in size between 0.1 mm and 0.5 mm in diameters (Fig. 6b and c). The grain dolostone/packstone are generally massive or trough or tabular cross-stratified, reflecting deposition in a relatively high energy environment. Dolomiticrite is common in the P₂l Formation, and is gray to dark gray in color, generally with over 80% micritic dolomite and additional minor feldspar and other components (Fig. 6e and f). Both massive and laminated dolomiticrite are common in the study area. With increasing content of terrigenous or tuffaceous clastic materials, silty or tuffaceous dolomiticrite and grain dolostone are developed, which are

dominated by dolomite (50–85%) and terrigenous or tuffaceous clastics (10–50%) (Fig. 6g and h). This development is a mixture of siliciclastics and micritic dolomite or intraclast, appearing as massive or laminated in structures. The micritic dolomite is generally subhedral to anhedral, while sparry dolomite is euhedral where the rim is seen as brighter than the mineral center on BSE images due to a higher iron concentration (Fig. 6d).

Tuffite is the most distinct rock type of the study area and is mainly present in the lower section (P₂l₁) of the P₂l Formation, with dark gray to black coloration (Fig. 6i, m). This lithofacies is identified from XRD data, mainly of siliceous, dominated by albite, K-feldspar, quartz, less carbonate and minor clay minerals (Fig. 6j and k). With increasing dolomite content, tuffite turns into dolomitic tuffite; with increasing terrigenous siliciclastics, tuffite turns into muddy or silty tuffite (Fig. 6l). Millimeter scale laminated tuffite is the most common

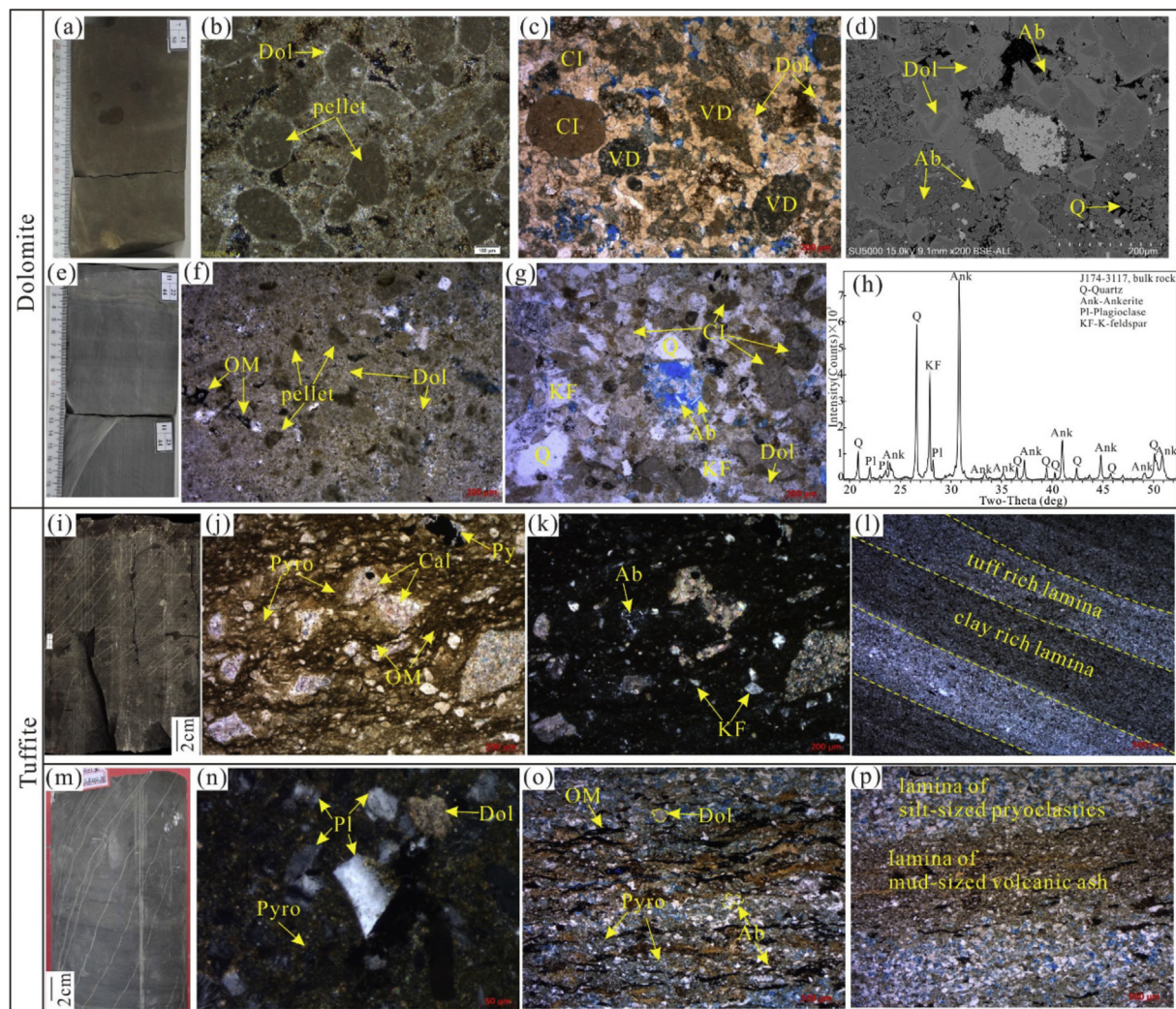


Fig. 6. Core photos and photomicrographs of dolomite and tuffite lithofacies. (a, b) Grain dolostone, gray in color, characterized by well-sorted and round pellets (J-174, 3152.46 m). (c, d) Round intraclasts and volcanic detritus with dominant rhomb-crystallized sparry dolomite and minor albite and quartz. The dolomite has brighter rim and darker center (J-30, 2-19). (e, f) Dolomicrite, gray to dark gray, is dominated by micritic dolomite (J-174, 3175.05 m). (g, h) Silty dolomite is composed primarily of dolomite, less quartz, albite and K-feldspar (J-174, 3117 m). (i–k) Dark gray tuffite, rich in pyroclasts and OM, has minerals as albite, K-feldspar with less calcite and dolomite (J-174, 3272.7 m). (l) Laminated muddy or silty tuffite comprising clay-rich lamina and tuff-rich lamina sharply superposed (J-174, 6-17). (m, n) Dark gray tuffite with poorly-sorted and subangular-angular particles (J-30, 3-45). (o, p) Laminated tuffite comprises lamina of silt-sized pyroclastics and lamina of mud-sized volcanic ash that are stacked with sharp contacts, with algae distributing along the bedding (J-37, 2844.1 m). VD–volcanic detritus, CI–carbonate intraclast, KF–K-feldspar, Ab–albite, Pl–plagioclase, Ma–matrix, Cal–calcite, Q–quartz, Pyro–pyroclast, Dol–dolomite, Ank–ankerite, OM–organic matter, Py–pyrite. (For interpretation of the references to color in this figure legend, the reader is referred to the Web version of this article.)

lithofacies, which is followed by massive tuffite lithofacies. Algae lamina, lamina of silt-sized pyroclastics and lamina of mud-sized volcanic ash are stacked with sharp or gradational contacts (Fig. 6l, o, p). Most of this lithofacies are characterized by relatively low compositional and textural maturity, containing poorly sorted fine and subangular particles (Fig. 6n). Because tuffites are dissolution-prone unstable volcanic materials, appreciable amounts of pore space is present in this lithofacies making tuffites a favorable reservoir unit.

4.2. Petrophysical properties and pore structures

4.2.1. Petrophysical properties

Petrophysical analyses show that the porosity and permeability of different lithofacies vary significantly (Fig. 7). It shows that dolomicrite (D) and mudstone (M) have the poorest petrophysical properties, with porosity ranging from 0.1% to 6.5% with mean value of 4.17% and permeability ranging from less than $0.01 \times 10^{-3} \mu\text{m}^2$ to $0.135 \times 10^{-3} \mu\text{m}^2$ with mean value of $0.03 \times 10^{-3} \mu\text{m}^2$. Therefore,

these dolomicrite and mudstone are hardly effective reservoirs. Dolomitic siltstone (D-S) has relatively narrow porosity and permeability range. The porosity of D-S ranges from 5% to 13% with average of 8.78%, and the permeability ranges from $0.005 \times 10^{-3} \mu\text{m}^2$ – $0.1 \times 10^{-3} \mu\text{m}^2$ with average of $0.06 \times 10^{-3} \mu\text{m}^2$. Tuffaceous siltstone (T-S) has relatively concentrated porosity and broad spreading permeability, ranging from 4% to 15% with mean value of 9.21% and $0.01 \times 10^{-3} \mu\text{m}^2$ to $0.5 \times 10^{-3} \mu\text{m}^2$ with high mean value of $0.36 \times 10^{-3} \mu\text{m}^2$. Tuffaceous dolomicrite (T-D) and silty dolomicrite (S-D) have relatively wide spreading petrophysical property values (Fig. 7). The porosity of T-D and S-D have relatively higher values with average of 10.33% and 10.09%, while the permeability of both lithofacies spread wide but with lower medium value of $0.025 \times 10^{-3} \mu\text{m}^2$ and $0.02 \times 10^{-3} \mu\text{m}^2$, respectively. Silty tuffite (S-T) is characterized by wide range of porosity and permeability, ranging from 0.5% to 27.8% (ave. = 10.84%) and $< 0.01 \times 10^{-3} \mu\text{m}^2$ to $9.17 \times 10^{-3} \mu\text{m}^2$ (ave. = $0.55 \times 10^{-3} \mu\text{m}^2$).

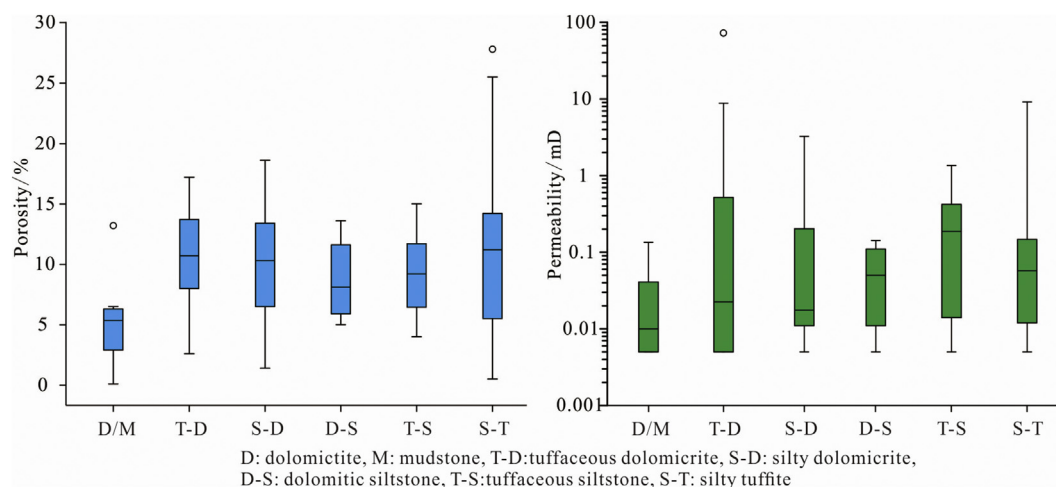


Fig. 7. Various porosity (a) and permeability (b) of different lithofacies in the P₂l mixed sedimentary rocks.

4.2.2. Pore characteristics

On the basis of microscopic and SEM analyses, the pore structures of the P₂l Formation mixed rocks appear to be complicated. There are mainly three pore types within the reservoirs: primary pores, secondary pores and fractures. Primary pores mostly comprise the remaining primary inter-granular pores after compaction, which commonly enlarged by dissolving into mixed pores and mainly existed in the silty grain dolostone (Fig. 8a). The remaining primary pores are relatively large with pore size of > 50 μm in diameter. Secondary pores are the most important reservoir space in the study area and developed almost in every lithofacies, especially fine sandstone/siltstones, silty grain dolostones and silty tuffite. Secondary pores are primarily intra-granular dissolving pores of feldspar (Fig. 8b) and debris (Fig. 8c) and inter-granular dissolving pores of pyroclastics (Fig. 8d and e) and minor carbonate (Fig. 8f). The secondary dissolving pores have wide size ranges, mainly from 3 μm to 100 μm, which are relatively smaller than the primary pores.

4.3. Element distribution patterns

4.3.1. Distribution of major and trace elements

The major and trace element results are listed in Table 1. SiO₂ is the predominant major element (oxide) in the P₂l Formation mixed sedimentary rocks, varying from 5.82% to 93.2% (ave. = 60.74%). The second most abundant oxide is CaO with contents ranging from 0.17% to 91.90% (ave. = 17.16%). The content of Al₂O₃ falls in between 0.81% and 15.25% (ave. = 9.27%), while the MgO content ranges from 0.88% to 19.60% (ave. = 5.71%). The average contents of the other major oxides are less than 5%, such as Fe₂O₃ (ave. = 3.96%), K₂O (ave. = 2.27%) and P₂O₅ (ave. = 0.52%). As shown in the upper continental crust (UCC) - normalized diagram (Fig. 9a), the mean concentrations of Si, Al, Ca, Mg, Na and Ti in silicate rich rocks are relatively higher, whereas K is relatively lower compared with those of the UCC (Taylor and McLennan, 1985, 1995). In dolomite-rich rocks, the average concentrations of Mg and Ca are obviously higher, whereas Si, Al, Fe, Na, K and Ti are lower than those of the UCC (Fig. 9b). For trace

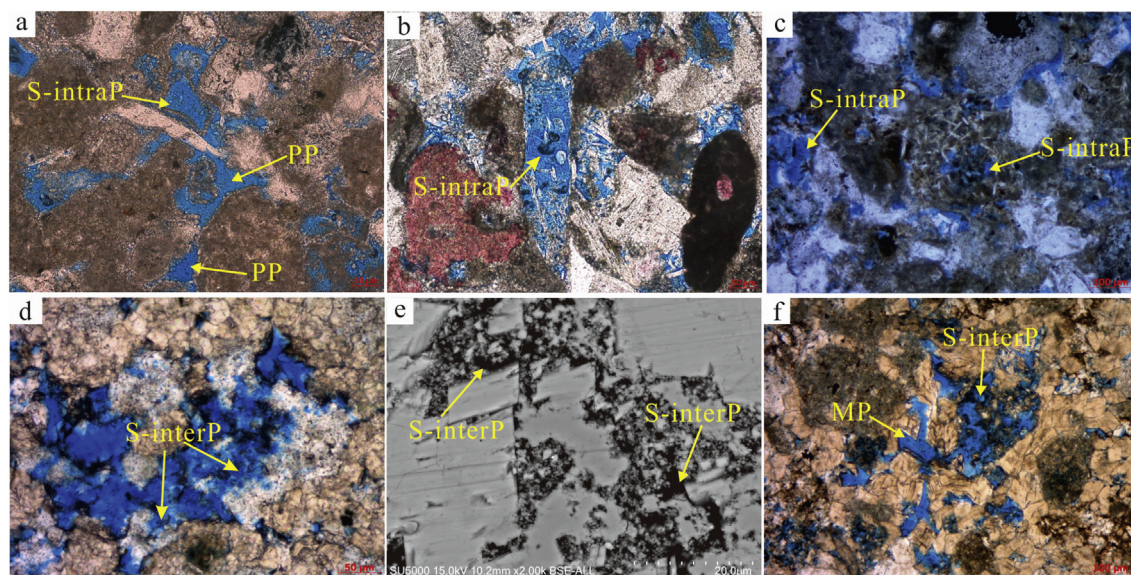


Fig. 8. Variety of pore types in the P₂l mixed sedimentary rocks. (a) Photomicrograph of primary pores and secondary intra-granular pores in silty grain dolostone (J-174, 3114.86 m). (b) Photomicrograph of feldspar dissolving pores in carbonate debris-rich fine sandstone (J-174, 3142.13 m). (c) Photomicrograph of secondary intra-granular pores by debris dissolving in dolomitic siltstone (J-251, 3596.82 m). (d) Photomicrograph of tuff dissolving pores in tuffaceous dolomictite (J-301, 2759.3 m). (e) BSE image of secondary inter-granular pores by dissolving of tuff in tuffaceous dolomictite (J-303, 2589.2 m). (f) Photomicrograph of mixed pores and secondary inter-granular pores, resulted from dolomite and tuff dissolution. PP—primary pores, MP—mixed pores, S-intraP—secondary intra-granular pores, S-interP—secondary inter-granular pores.

Table 1
Chemical compositions of the P₂l mixed sedimentary rocks in the Jimusar Sag.

Sample	SiO ₂	Al ₂ O ₃	Fe ₂ O ₃	MgO	CaO	Na ₂ O	K ₂ O	MnO	TiO ₂	P ₂ O ₅	LOI	CIA	Li	Be	Sc	V	Cr	Co	Ni
J-1	58.8	13.77	3.25	2.47	3.29	5.42	2.68	0.034	0.582	0.118	9.53	46	55.4	1.89	5.59	77.8	53.3	6.72	52.3
J-2	56.84	12.91	3.32	2.55	5.48	4.69	2.88	0.069	0.459	0.181	10.49	43	64.8	1.66	9.56	69.6	41	12	46.2
J-3	54.35	10.46	3.3	1.74	4.89	2.84	2.22	0.033	0.508	1.27	18.33	49	94.6	1.85	12.7	86.8	50.6	12	110
J-4	7.9	0.733	3.42	17.47	26	0.432	0.149	0.169	0.039	0.063	43.58	33	12	1.08	9.62	104	14.4	2.81	68.6
J-5	19.08	4.53	2.48	12.18	18.92	1.35	1.6	0.07	0.21	0.09	39.43	44	42.8	0.812	13.3	110	20.7	7.24	56.6
J-6	32.98	2.82	1.83	11.8	17.44	1.05	0.804	0.133	0.134	0.047	30.93	41	33.4	0.835	17.2	78.1	21	3.71	80.9
J-7	62.56	13.91	4.69	1.52	0.885	3.65	4.25	0.068	0.502	0.074	7.82	55	101	1.06	14.2	56.1	38.9	7.35	45
J-8	21.22	0.711	2.65	12.97	25.34	0.253	0.121	0.146	0.029	0.038	36.5	44	11.2	0.469	1.75	26.6	261	5.29	128
J-9													135	2.07	11.6	80.5	294	10.4	117
J-10	53.92	8.83	4.09	6.84	7.3	2.57	2.26	0.107	0.296	0.08	13.68	47	116	2.32	10.7	95	43.6	8.1	33.6
J-11	54.36	11.27	2.95	3.59	8.73	5.14	1.46	0.086	0.387	0.235	11.73	40	60.9	1.43	9.45	53.6	94.4	9.15	58.9
J-12	57.09	11.75	5.32	1.62	5.43	2.96	3.51	0.066	0.592	0.317	11.18	48	56	1.74	5.92	90.4	127	13.2	103
J-13	33.83	4.93	2.3	6.85	15.18	1.79	1.04	0.095	0.306	0.11	33.55	43	312	0.931	8.85	94.7	21.5	9.58	61.5
J-14	2.96	0.448	1.32	12.97	36.49	0.296	0.067	0.279	0.022	0.096	45.04	32	11.2	0.931	5.47	50.7	6.34	3.26	40.8
J-15	31.1	4.94	2.92	9.86	19.11	2.44	0.597	0.152	0.226	0.063	28.56	27	12	1.43	3.87	49.5	363	6.48	179
J-16	38.82	8.7	4.23	6.16	14.49	3.75	1.41	0.186	0.256	1.05	20.91	25	9.84	2.2	23.9	40.8	22.9	6.38	35
J-17	35.56	1.09	2.76	11.72	19.08	0.381	0.19	0.128	0.024	0.073	28.96	67	49.8	0.484	6.82	46	8.49	1.71	24.8

Sample	La	Ce	Pr	Nd	Sm	Eu	Gd	Tb	Dy	Ho	Er	Tm	Yb	Lu	Total REE	HREE	LREE	LREE/HREE
J-1	18.6	38.9	5.18	21.3	4.61	0.729	3.75	0.713	3.41	0.657	1.66	0.277	1.75	0.235	101.771	4.579	83.98	18.34
J-2	35.8	76.6	9.48	39.6	8.27	1.21	6.91	1.14	5.16	0.965	2.69	0.449	2.87	0.424	191.568	7.398	161.48	21.83
J-3	20.7	41.4	5.5	22.8	4.63	0.841	4	0.764	4.12	0.864	2.61	0.525	3.82	0.645	113.219	8.464	90.4	10.68
J-4	3.32	5.94	0.743	3.04	0.676	0.25	0.591	0.111	0.691	0.161	0.458	0.079	0.579	0.084	16.723	1.361	13.043	9.58
J-5	20.4	49.1	6.85	31.4	6.63	1.04	5.24	1.11	6.37	1.48	4.32	0.92	6.38	0.965	142.205	14.065	107.75	7.66
J-6	14.6	34.2	4.06	17.1	3.45	0.61	3.08	0.579	3.22	0.721	2.11	0.421	2.74	0.398	87.289	6.39	69.96	10.95
J-7	22.2	44.8	5.55	23.6	5.31	0.801	4.7	0.988	5.98	1.31	3.73	0.723	4.52	0.657	124.869	10.94	96.15	8.79
J-8	5.17	16.3	2.02	9.69	2.42	0.55	2.37	0.585	4.06	0.964	2.7	0.517	2.9	0.4	50.646	7.481	33.18	4.44
J-9	22.8	48.3	5.93	23.4	5.17	0.853	4.85	1.03	6.36	1.38	3.54	0.625	3.68	0.511	128.429	9.736	100.43	10.32
J-10	17.2	34.8	4.19	16.4	3.45	0.606	2.97	0.577	3.26	0.669	1.98	0.367	2.36	0.344	89.173	5.72	72.59	12.69
J-11	24	51.1	6.55	27.8	6.15	0.934	5.37	1.13	6.51	1.38	3.67	0.676	3.9	0.528	139.698	10.154	109.45	10.78
J-12	18.5	37.3	4.77	19.4	4	0.728	3.51	0.649	3.48	0.683	1.77	0.289	1.63	0.231	96.94	4.603	79.97	17.37
J-13	16.5	34.8	4.46	19.4	4.41	0.719	4.01	0.774	4.28	0.884	2.34	0.443	2.99	0.467	96.477	7.124	75.16	10.55
J-14	7.08	20.3	2.58	11.7	3	0.624	2.82	0.712	5.07	1.18	3.35	0.659	3.74	0.529	63.344	9.458	41.66	4.40
J-15	27.6	52.6	6.44	25.8	5.26	0.601	4.19	0.667	2.74	0.463	1.2	0.15	0.912	0.112	128.735	10.434	118.301	11.34
J-16	24.4	56.6	7.56	33.2	8.07	1.45	7.33	1.69	11.2	2.48	6.44	1.23	6.84	0.928	169.418	38.138	131.28	3.44
J-17	4.71	13.3	1.38	6.15	1.43	0.285	1.3	0.301	1.96	0.47	1.46	0.295	1.94	0.288	35.269	8.014	27.255	3.40

Sample	Cu	Zn	Ga	Rb	Sr	Y	Mo	Cd	In	Sb	Cs	Ba	Th	U	Nb	Ta	Zr	Hf	Rb/Sr
J-1	23.7	71	18.3	59.8	171	90.2	3.01	0.112	0.063	0.243	3.56	325	3.49	1.33	9.56	0.748	1558	35.6	0.350
J-2	25.8	93.4	17.9	64.8	609	81.9	2.91	0.144	0.077	0.894	2.34	435	4.96	1.57	8.4	0.843	1233	27.8	0.106
J-3	47.4	152	12.7	71.4	608	272	4.25	0.198	0.055	1.28	5.12	427	5.05	5.63	7.77	0.552	5102	114	0.117
J-4	13.1	23.4	1.14	4.56	1151	24.8	1.39	0.033	0.003	0.092	0.14	379	0.295	0.656	0.522	0.054	379	9.28	0.004
J-5	40.6	41.1	5.36	26.3	1003	71.9	14.2	0.232	0.031	0.463	1.32	460	10.1	3.84	2.99	0.233	462	11.5	0.026
J-6	127	49.5	3.17	14.5	1163	129	3.56	0.237	0.016	0.471	0.732	346	2.99	3.57	1.8	0.125	2225	49.7	0.012
J-7	57.2	49.1	8.15	20.6	1041	61	1.46	0.059	0.021	1.06	1.73	381	4.61	3.56	5.35	0.411	559	14.5	0.020
J-8	8.17	12.7	1.25	3.14	453	55	1.78	0.04	0.005	0.584	0.079	411	1.74	0.611	0.432	0.033	472	11	0.007
J-9	74.7	71.8	12.4	60.6	707	58.2	3.19	0.117	0.045	0.604	2.85	374	2.77	2.95	8.29	0.637	595	15.2	0.086
J-10	421	106	14.4	89.2	441	20.2	1.76	0.103	0.083	0.427	4.86	326	3.24	1.84	10.2	0.737	200	5.78	0.202
J-11	30.2	76.8	14.1	41.8	559	64.7	3.37	0.125	0.059	1.06	2.56	320	7.47	3.37	6.81	0.697	651	17.2	0.075
J-12	48.7	68.9	14.3	81.3	282	107	4.35	0.131	0.059	1.05	8.52	408	5.46	1.95	8.15	0.52	1862	42.6	0.288
J-13	46.8	54.6	6.49	43.3	755	57.9	4.97	0.231	0.026	0.436	2.97	223	5.26	2.93	5.71	0.286	696	17.3	0.057
J-14	243	18.9	1.36	6.71	1846	39.7	0.585	0.016	< 0.002	0.155	0.154	522	3.01	1.64	0.425	0.075	38.6	0.341	0.004
J-15	27.9	75.5	16.1	81.5	138	46	2.98	0.1	0.062	0.338	2.08	266	2.66	0.376	8.29	0.888	693	18.2	0.591
J-16	24.8	50.8	9.62	34.3	686	78.8	0.72	0.143	0.052	0.863	1.06	768	13.2	5.01	5.15	0.465	128	3.84	0.050
J-17	1070	22.1	1.84	6.95	675	15.6	0.389	0.078	< 0.002	0.087	0.239	205	1.12	1.24	0.561	0.072	60.6	1.54	0.010

Note: major oxides reported with wt%, trace elements reported with ppm. LOI = loss on ignition; CIA = chemical index of alteration; REE = rare earth elements; LREE = light rare earth elements; HREE = heavy rare earth elements.

elements, V, Cr, Ni, Cu, Sr, Zr, Hf and Y show marked enrichment on average in both rock types, whereas Sc, Co, Rb, Ba, Th, U and Nb are generally lower compared with those of the UCC (Taylor and McLennan, 1995) (Fig. 9a and b).

The concentrations of major and trace elements in sedimentary rocks are mainly controlled by terrigenous clastics input, biogenic deposit and sedimentary and diagenetic processes (Murray and Leinen, 1993; Bach and Irber, 1998). R hierarchical cluster analysis using the IBM SPSS statistics 18 program was applied to distinguish the different processes and influencing factors. The outcome of this method is a number of clusters where the data within a cluster are similar, while the differences between the clusters are as large as possible. Two primary

element groups are obtained from the R-mode cluster analyses. The first group (Group I) includes the representative elements Zr, Ti, Cu, Cr, Ni and Th. Organic matter related phosphorous (P), high-field strength elements (including Mo, Th, Ti and Rb) and some other elements (Cu and V, Zn) are also clustered into Group I. The second group (Group II) is characterized by some lithophile elements (Mn, Ba, Cs, Sr and Sc).

The content of major and trace elements in the P₂l Formation vary significantly as they include felsic (Al, Si, K) and carbonate minerals (Ca, Mg), redox sensitive parameters (Mo, V, U, Mn and S), paleosalinity (Cl, Sr/Ca, Sr/Ba) and paleo-climate parameters (Cu, Sr, Mn and Rb/Sr). The conspicuous linear relationships between SiO₂, K₂O and Na₂O with Al₂O₃ (Fig. 8a, b, c) suggest that the minerals hosting Si,

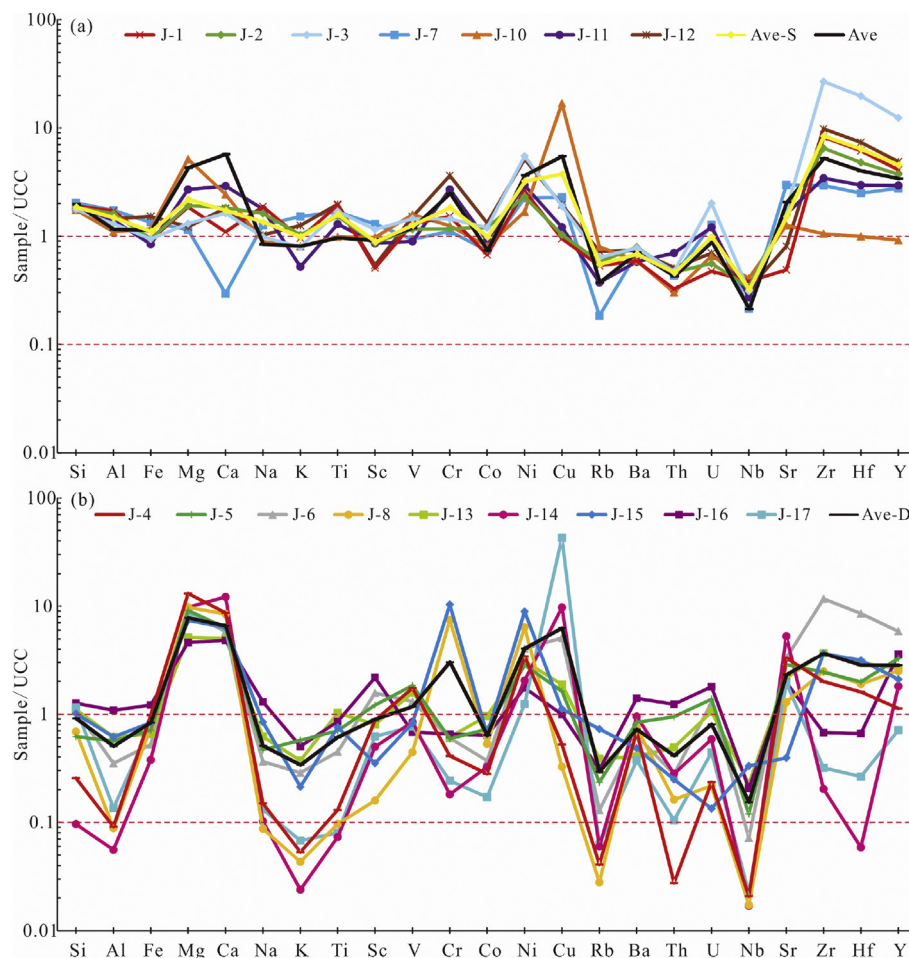


Fig. 9. UCC-normalized diagrams of multi elements for (a) silicate-rich rocks and (b) dolomite-rich rocks in the P_{2l} mixed sedimentary rocks in the Jimusar Sag (Taylor and McLennan, 1995). The yellow line (Ave-S) in (a) represents the average of element content of the silicate-rich samples, the black line (Ave) is the average of all the studied samples. The black line (Ave-D) in (b) represents the average of dolomite rich rocks. (For interpretation of the references to color in this figure legend, the reader is referred to the Web version of this article.)

Na, K and Al are mainly K-feldspar and albite. The deviated points (within the dashed circle in Fig. 10a) from the main linear relation are attributed to the Si hosted in quartz. The negative correlation of CaO and MgO with Al_2O_3 (Fig. 10d and e) suggest that the CaO and MgO are mainly hosted in carbonate minerals, while Al_2O_3 are hosted within aluminosilicate minerals. The points within the dashed circle in Fig. 10d show relatively less CaO comparing to the main tendency, these points probably represent rocks that have more content of other minerals hosting less CaO rather than carbonate minerals, such as zeolite or montmorillonite. The obvious positive linear correlation between CaO and MgO indicates that these elements are mainly hosted within dolomite, while a small number of points (in the dashed circle in Fig. 10f) with low MgO contents suggest rocks containing more calcite than dolomite. TiO_2 and Al_2O_3 contents vary in the study rocks and display a positive correlation with a TiO_2/Al_2O_3 slope of 0.0642 ($R^2 = 0.6235$) (Fig. 10g). Some of the elements and element ratios show conspicuous correlations including (1) a positive relationship between Al_2O_3 content and Cr content, (2) a negative relationship between Rb/Sr and Sr/Ba, (3) a positive correlation between Sr/Ba and CaO, (4) a negative relationship between Rb/Sr and MgO and (5) a positive correlation between Sr and Mn (Fig. 10h, i, j, k, l) contents. This indicate that the paleo-environmental settings including sediment input, redox processes, paleosalinity and paleoclimate can be viewed as a coupled system, where the elements could be used to detect and reflect paleo-environment.

4.3.2. Vertical distribution of geochemical parameters

Results show that the Rb/Sr ratio within the P_{2l} Formation varies between 0.002 and 3.21 (ave. = 0.20), and the content of Mn varies from 0.014 to 0.79% (ave. = 0.10). The Rb/Sr ratios increase upward from the basal section of the formation (Fig. 11). The Sr/Ba ratio of P_{2l} samples ranges from 0.04 to 11.30 (ave. = 1.06), higher in the P_{2l1}^2 and P_{2l2}^2 intervals and relatively lower in the P_{2l1}^1 interval, while the MgO content (ave. = 5.71) varies similar to the Sr/Ba ratio (Fig. 11). The ratio of Th/U is negatively proportional to reduction condition and indicates anoxic condition with a ratio less than 1.33 (Zhang et al., 2016). The range of Th/U ratio is from 0.35 to 5.37 (ave. = 1.14) within the P_{2l} Formation, relatively higher in the P_{2l1}^1 interval but lower in the P_{2l1}^2 and P_{2l2}^2 intervals. The content of pyrite and TOC content are inversely correlated with the Th/U ratio profile (Fig. 11).

4.3.3. REE and the chondrite- and primitive mantle-normalized patterns

The total REE content in the P_{2l} Formation range from 16.72 to 191.57 ppm, with an average of 104.46 ppm, which is lower than those of the upper continental crust (UCC) (average 146.37 ppm) but higher than those of the lower continental crust (LCC) (average 66.98 ppm) (Taylor and McLennan, 1985). The Light Rare Earth Elements (LREE) (La–Eu) contents and Heavy Rare Earth Elements (HREE) (Gd–Lu) contents fall in 13.97–170.96 ppm (average 87.34 ppm), and 2.75–38.14 ppm (average 17.12 ppm), respectively. The LREE/HREE ratio ranges from 2.49 to 11.34, with an average of 5.38 (Table 1), indicating that these samples are relatively enriched in LREE. The

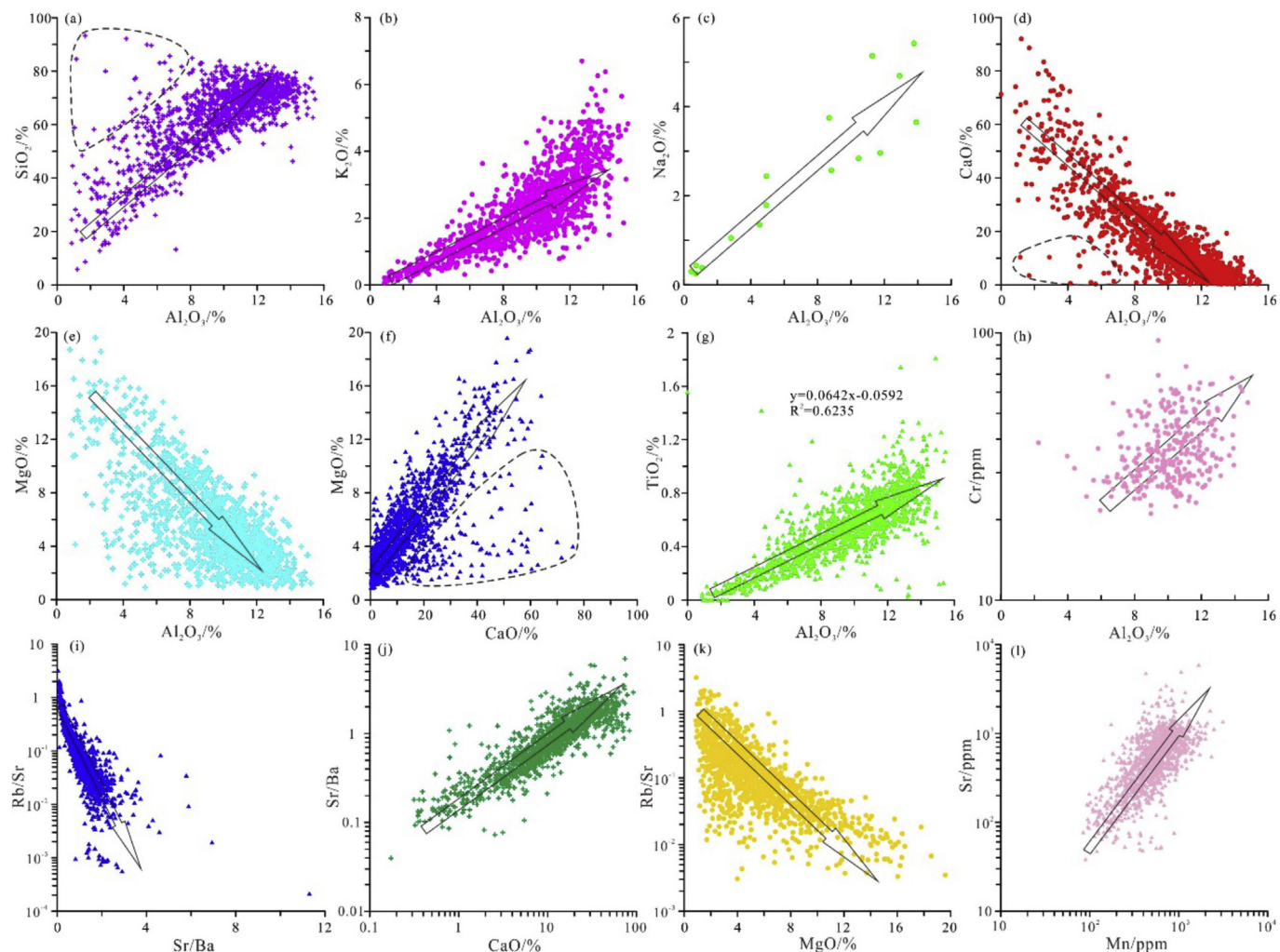


Fig. 10. Distribution patterns of major and trace elements and ratios of the P_{2l} Formation showing conspicuous correlations between (a) Al₂O₃ content and SiO₂ content, points within the dashed circle are deviated from the main linear relation, attributed to the Si hosted in quartz. (b) Al₂O₃ content and K₂O content, (c) Al₂O₃ content and Na₂O content, (d) Al₂O₃ content and CaO content, points within the dashed circle show relatively less CaO comparing to the main tendency, these points probably represent rocks that have more content of minerals hosting less CaO than carbonate minerals. (e) Al₂O₃ content and MgO content, (f) CaO content and MgO content, a small number of points in the dashed circle with low MgO contents suggest rocks containing more calcite. (g) Al₂O₃ content and TiO₂ content, (h) Al₂O₃ content and Cr content, (i) Sr/Ba ratios and Rb/Sr ratios, (j) CaO content and Sr/Ba ratios, (k) MgO content and Rb/Sr ratios, (l) Mn content and Sr content.

chondrite-normalized and primitive mantle-normalized REE distribution patterns of the P_{2l} mixed sedimentary rocks show similar tendency and are generally right inclined (Fig. 12), also revealing significant enrichment of LREE and depletion in HREE. An obvious negative Eu anomaly is also shown in the chondrite-normalized pattern (Fig. 12a and b).

5. Discussion

The TOC of the studied samples range from 0.05 to 15.51%, with an average of 3.03% showing that many sections within the P_{2l} Formation are potentially good source rocks. The vitrinite reflectance (Ro) is ranging from 0.76 to 1.04%. Mongenot et al. (1996) suggested that thermal evolution and maturity of an OM-rich formation has no detectable effects on the distribution of trace elements. This means that the trace elements could be used as reliable paleo-environmental proxies.

5.1. Provenance

The mixed sedimentary rocks of the P_{2l} Formation in the Jimusar Sag have three principal sources: terrigenous clastics, pyroclastic

components and autochthonous to parautochthonous carbonates. The carbonate rocks, which are mainly deposited from autochthonous to parautochthonous carbonate components, can be easily distinguished by their high content of Ca and Mg elements. Both the siltstone/sandstones and tuffaceous sedimentary rocks show siliciclastic mixture of terrigenous clastic and pyroclastic components to various degrees and also minor carbonate content. It is difficult to differentiate the pyroclastics from terrigenous siliciclastics just using some traditional methods, such as XRD and microscopic observation. Therefore, elemental and geochemical data, which could reflect the provenance characters, are applied to help study the mixed sedimentary rocks.

The similar shaped curves showing relatively high LREE/HREE ratios and obvious negative Eu anomaly (Fig. 12) indicate that the silicate minerals have similar REE origin and are sourced from felsic rocks as terrigenous and tuffaceous substances (Taylor and McLennan, 1985; Kasanzu et al., 2008).

The first group (Group I) derived from the R-mode cluster analysis mainly characterizes the terrigenous input from outside the lake basin, such as the representative elements Zr, Ti, Cu, Cr, Ni and Th. The other elements in Group I like phosphorous (P) could reflect the volcanic input (Peng et al., 2012), and the high-field strength elements including Th, Ti and Rb are associated with clay and rock-forming minerals (Xie

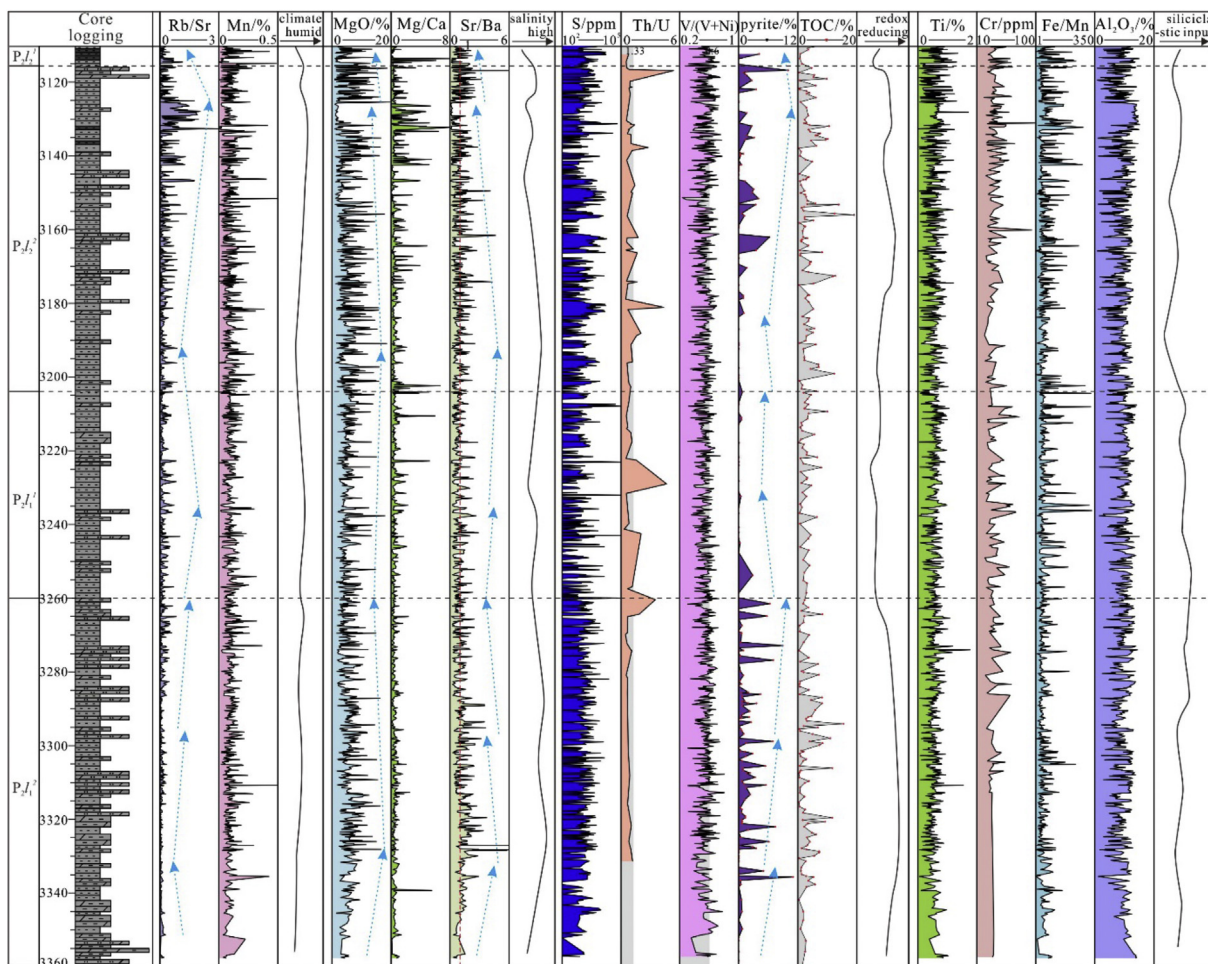


Fig. 11. Sedimentary environmental settings of the P₂l mixed sedimentary rocks, evidenced by chemostratigraphic parameter profiles from Well J-174.

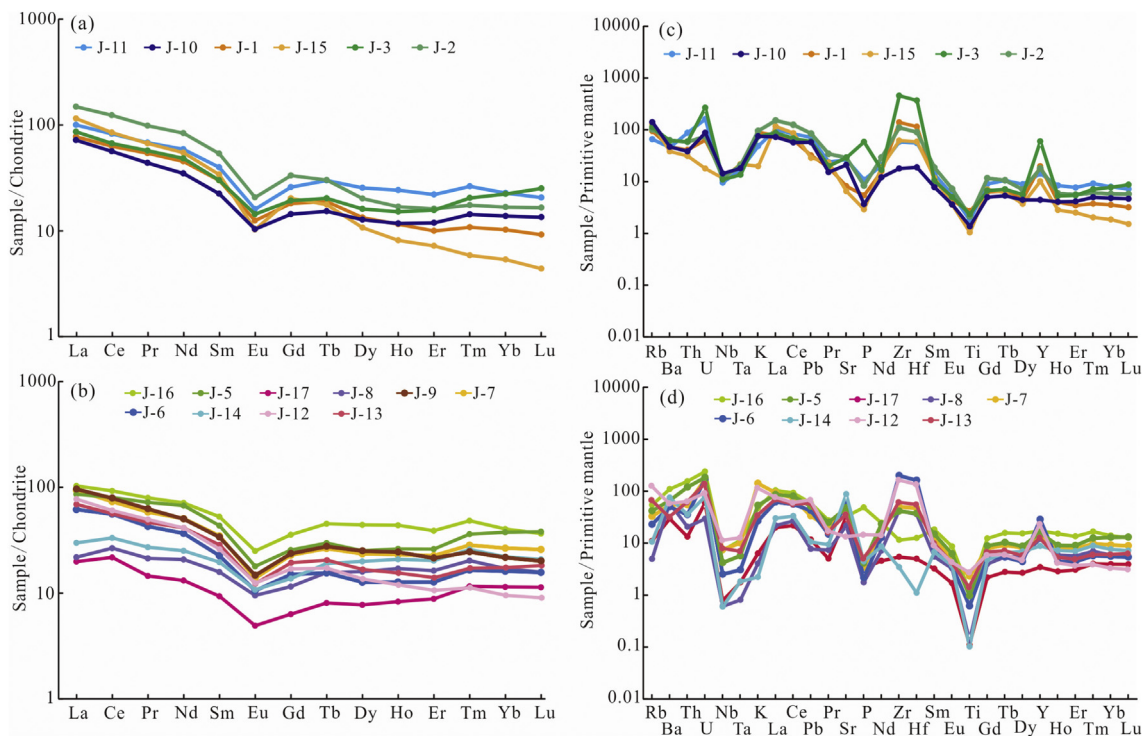


Fig. 12. Chondrite-normalized and primitive mantle-normalized REE distribution patterns of silicate rich rocks (a, c) and carbonate rich rocks (b, d) from the P₂l mixed sedimentary rocks.

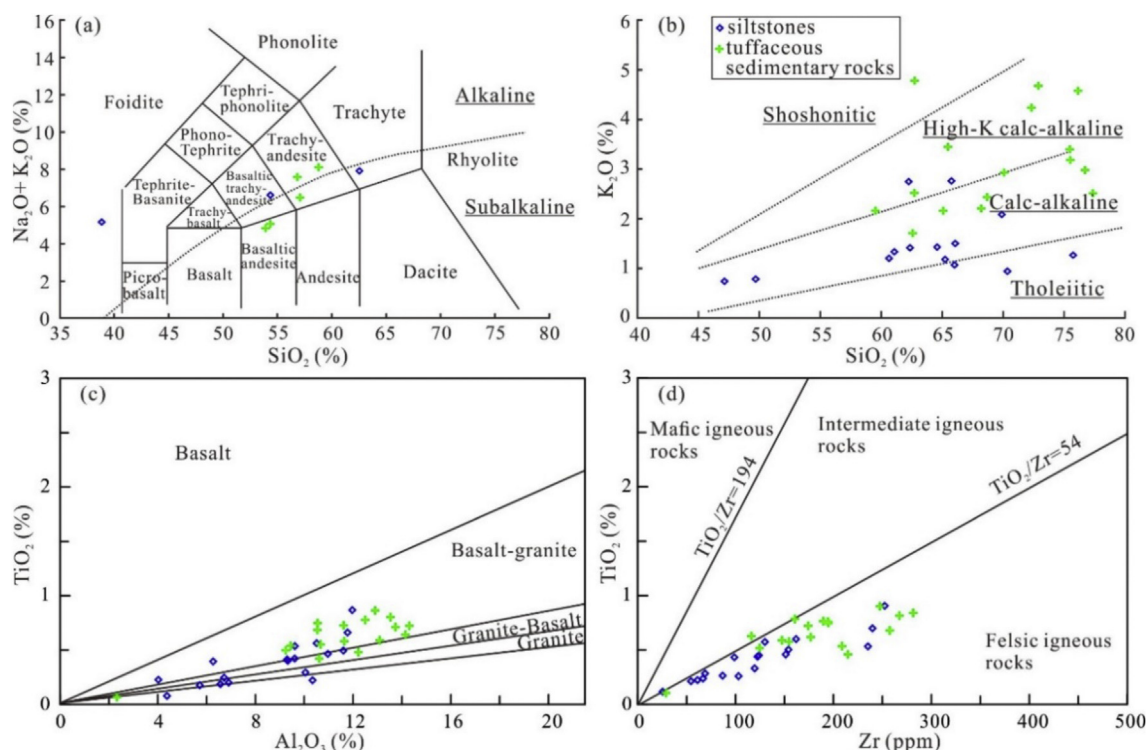


Fig. 13. Provenance discrimination. (a) TAS-total alkalis ($\text{Na}_2\text{O} + \text{K}_2\text{O}$) vs. SiO_2 after Maitre (1989). (b) Total K_2O vs. SiO_2 after Rickwood (1989). (c) Bivariate diagram for Al_2O_3 vs. TiO_2 . (d) Bivariate diagram for Zr vs. TiO_2 .

et al., 2018) and elements like S, Cu and V could reflect the depositional environment. Overall, the elements within Group I are associated with source rock properties and depositional environments. The second group (Group II) derived from the R-mode cluster method features elements which are part of geochemical products formed within the lake basin, with representative elements including Ba, Mn and Sr. In this way, the elements in Group II is closely related to the chemical properties of water (Peng et al., 2012).

The TAS-total alkalis ($\text{Na}_2\text{O} + \text{K}_2\text{O}$) vs. SiO_2 diagram (Maitre, 1989) (Fig. 13a) shows that most of the components in both sandstone/siltstones and tuffaceous rocks are derived from an intermediate-subalkaline source. Subdivision of subalkalic rocks using a K_2O vs. SiO_2 diagram according to Rickwood (1989) (Fig. 13b) shows that the siltstone/sandstones are mainly sourced from calc-alkaline series of rocks and the tuffaceous sedimentary rocks belong to the high-K calc-alkaline series rocks.

Most of the elements, especially Ca, Mg, K and Na, are partly leached out during weathering of the original rocks found in different source areas, whereas elements, such as Ti, Zr and Al, are more immobile, because of their low solubility in aqueous solutions (Wesolowski, 1992; Zhou et al., 2015). Therefore, the Ti/Al and Zr/Al ratios of sedimentary rocks may be used as indicators of provenance properties (Zhou et al., 2015). Previous studies have shown that the weight ratio of $\text{Al}_2\text{O}_3/\text{TiO}_2$ found in sediments retain the original provenance rock values. Ratios within the range of 3–8 suggests original mafic igneous rocks, ratios with the range of 8–21 represent intermediate igneous rocks, while ratios higher than 21 represent felsic igneous rocks (Hayashi et al., 1997; Zhou et al., 2015). Fig. 13c shows a linear relationship between TiO_2 and Al_2O_3 , and the $\text{Al}_2\text{O}_3/\text{TiO}_2$ ratios are essentially between 14 and 25 for the siltstones and tuffaceous sedimentary rocks, which mostly fall into the range of intermediate igneous rocks and partly in the felsic rock field. The TiO_2/Zr weight ratios fall mostly in the felsic igneous rocks field, with some samples falling into the intermediate igneous rock field in the TiO_2 vs. Zr diagram (Fig. 13d), but within the intermediate igneous rock field on the basis of

their $\text{Al}_2\text{O}_3/\text{TiO}_2$ ratios diagram. This feature was also documented by Hayashi et al. (1997), and was attributed to the significant fractionation of zircon during clastic sediments transportation and deposition (Argat and Donnelly, 1987). There are no significant spatial and temporal variations among the provenance sensitive ratios of the studied samples, which reflect a common intermediate source rock for the P₂l mixed sedimentary rocks.

Previous studies have shown that phosphorus found in the fine-grained sedimentary rocks are sensitive to the changing paleo-conditions and are closely related to organic matter (Haskin and Haskin, 1966; Peng et al., 2012). Phosphorus provide nutrition and promote algae blooming, while at the same time leading to the formation of anoxic and reducing condition, further enhancing organic matter preservation (Wang et al., 2013). Phosphorus are significantly enriched in the studied samples (Fig. 14), compared to the mudstones of the P₂l Formation located in the northern Bogeda Mountain (average of 0.17) (Li, 2009). The samples from the Bogeda Mountain are mainly mudstones without tuffaceous materials. The correlation between

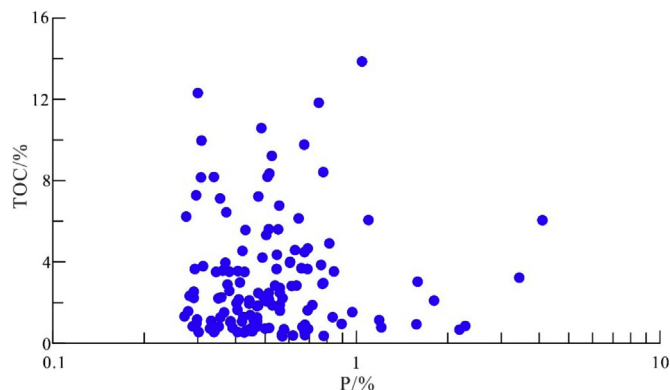


Fig. 14. Relationship between TOC and phosphorus content, showing high content of phosphorus and poor correlation between TOC and phosphorus.

phosphorus content and TOC in Fig. 14 is not linear, which is most likely caused by input of volcanic ash from surrounding volcanos (Peng et al., 2012).

5.2. Depositional environmental setting

5.2.1. Paleo-climate

The physical and chemical environment settings during deposition in lacustrine sedimentary systems may influence the element distribution in sediments. The element distribution is found to be closely related to paleo-climate (Tanaka et al., 2007; Meng et al., 2013). The chemical index of alteration (CIA, (Nesbitt and Young, 1982)), calculated from equation (1), is widely applied to determine the paleo-weathering of sediments and reflect the paleo-climate conditions (McLennan, 1993; Bock et al., 1998; Riebe et al., 2004).

$$\text{CIA} = [\text{Al}_2\text{O}_3 / (\text{Al}_2\text{O}_3 + \text{CaO}^* + \text{Na}_2\text{O} + \text{K}_2\text{O})] \times 100 \quad (\text{all in molar proportions}) \quad (1)$$

The CaO^* only represents the CaO content related with silicates, which is determined by expression $\text{CaO}^* = \text{CaO} - (10/3 \times \text{P}_2\text{O}_5)$ corrected for phosphate using P_2O_5 . If the remaining CaO mole fraction is greater than Na_2O , then CaO^* is considered equal to Na_2O ; otherwise, molar proportion of CaO is CaO^* (McLennan, 1993).

Besides the carbonate rock samples (J4, J6, J14, J15, J16), the low CIA values (40–67) (Table 1) show that both siltstone/sandstones and tuffaceous mixed sedimentary rocks were deposited under relatively dry paleo-climate conditions during low chemical weathering (the average upper crust has a CIA value of about 47) (McLennan, 1993; Bock et al., 1998; Bai et al., 2015).

In addition, some trace elements and their ratios are also sensitive to paleo-climate. Generally, Cu, Sr, Ba and Mn are precipitated and increased during arid conditions, while elements of Fe, Al, V, Ni, Zn and Co are relatively increased during humid conditions (Wang and Zhang, 1996; Bai et al., 2015; Ma et al., 2016b). The studied samples have relatively low Rb/Sr values ranging from 0.004 to 0.59 (Table 1) with an average of 0.12 from WD-XRF, and primarily ranging from 0.002 to 0.9 with an average of 0.17 from pXRF. The low Rb/Sr ratio values indicate warm and arid conditions (Jin and Zhang, 2002), which is consistent with the results from CIA values. Tuffaceous mixed sedimentary rocks has Rb/Sr ratio values ranging from 0.003 to 1.58 with an average of 0.42, and siltstone/fine sandstones has Rb/Sr values between 0.01 and 0.16 with an average of 0.052; while the Rb/Sr ratio of the dolomite lithofacies is 0.08–0.34 with an average of 0.083, and fine-grained sediments rich in calcite has Rb/Sr values ranging from 0.07 to 0.22 with an average of 0.068 (Fig. 15a, c). Based on Rb/Sr ratios, the carbonate rocks with lower Rb/Sr values were generally deposited during warm and arid conditions, while fine-grained clastic sediments were deposited during more humid conditions with higher Rb/Sr values. The low Rb/Sr values of siltstone/fine sandstones and fine-grained sediments are highly likely due to the presence of carbonate minerals in these rocks, decreasing the rocks bulk Rb/Sr ratio (Fig. 15a, c).

The Sr/Ba ratio is also regarded as an indicator for paleo-salinity (Drummond et al., 1993). The Sr/Ba values distribution of the studied samples (Fig. 15b and c) shows that only some of the tuffaceous mixed sedimentary rocks have relatively lower Sr/Ba values (less than 0.6), suggesting fresh water deposition; most of the carbonate-related samples, however, have Sr/Ba greater than 0.6, or even greater than 1, indicating deposition in brackish to salt water (Drummond et al., 1993).

5.2.2. Paleo-redox conditions

The trace elements of Th, U, V, Ni, Cr and Co and their ratios are considered as indicators of redox conditions (Hayashi et al., 1997; Pollack et al., 2009; Liu et al., 2018). Reduced conditions are featured by the value of Th/U ratio less than 1.33, V/Cr higher than 4.25 and V/(V+Ni) higher than 0.84; whereas relatively oxic conditions are

indicated by Th/U higher than 1.33, V/Cr less than 2 and V/(V+Ni) less than 0.6 (Jones and Manning, 1994; Xu et al., 2017; Xie et al., 2018).

The V/(V+Ni) ratio values, ranging from 0.32 to 0.8 with an average of 0.55 (Fig. 16), generally indicate dysoxic to anoxic conditions for these sedimentary rocks, but sometimes may also be indicative of oxic conditions (Xie et al., 2018; Xu et al., 2017). Both the P_{21} interval with Th/U (0.35–4.67, avg. 1.09), V/Cr (1.08–7.17, avg. 3.31) and V/(V+Ni) (0.31–0.81, avg. 0.55) and the P_{22} interval Th/U (0.52–5.37, avg. 1.17), V/Cr (0.89–7.67, avg. 3.32) and V/(V+Ni) (0.24–0.78, avg. 0.56) were under reduced and anoxia depositional conditions. The vertical distribution and variation of the trace element contents, ratio values and TOC (Fig. 11) show that the redox condition frequently changed during the deposition of the P_{21} mixed sedimentary rocks. Oxic, dysoxic and anoxic conditions are all suggested by the data but overall were dominated by anoxic and specially dysoxic depositional conditions.

The bacterial sulfate reduction (BSR) forming H_2S for pyrite is accomplished by organic matter oxidation (Bernier and Raiswell, 1983; Zhou et al., 2015). Therefore, there is a positive relationship between TOC and S. The TOC, as well as P, and S contents show relatively similar trends in the studied samples (Fig. 17). In muddy or silty tuffaceous mixed sedimentary rocks, the TOC and S contents are relatively higher than in the carbonate and sandstones rich rocks, which indicate that the muddy or silty tuffaceous mixed rocks were deposited during more reducing conditions.

5.3. Effect of sedimentary environmental setting

5.3.1. Effect of sedimentary environmental setting on lithofacies

Climate changes affected weathering, sediment supply and lake level fluctuation. Provenance changes and also active volcanism resulted in the mixed sedimentary rocks. The mineral composition and lithofacies are controlled by the above mentioned factors changing the sedimentary environments, and therefore the changes in compositions and lithofacies.

Three typical lithofacies associations and shifts of depositional environments can be seen from the parameters shown in Fig. 18 as a function of two different burial depth intervals in Well J-174.

- (1) Fig. 18a from the lower part of the upper core interval (3124.5–3130 m) of Well J-174 show higher Si, Al and K contents and lower Ca and Mg, reflecting detrital clastics such as feldspar, quartz and clay minerals. The relatively lower Sr/Ba ratios found in this interval indicate low paleo-salinity, ranging from fresh water to brackish water conditions. The high Rb/Sr ratios, V and S concentrations, along with low Cu and Mn concentrations, indicate humid and reducing conditions. The presence of relatively high Ti content and Ti/Al ratio reflects growing supply of clastics. Combined with core observations these data show that the lower part mainly contain superposed muddy or silty tuffite thin layers. Comparatively the upper part of the lower core interval (3121–3124.5 m) has higher Ca and Mg contents and lower Si, Al and K contents, indicating increased carbonate minerals deposition and lower detrital clastics input. Compared to the lower part of the core interval, there appears to be increased Sr/Ba ratios, Cu and Mn concentrations, sharply decreased Rb/Sr ratios and Ti contents, suggesting increasing paleo-salinity, weakly arid climate and a relative increase in oxic conditions. The high frequency variation seen in the curve represents rapid changes of lithofacies and depositional environments, resulting in interbedded micritic dolomite and dolomitic tuffite.
- (2) Fig. 18b, the lower part of the lower core interval (3146–3150 m) from Well J-174, comprises mainly alternating muddy tuffite and silty dolomite deposits. The muddy tuffite corresponds to relatively higher Si, Al and K contents and lower Ca and Mg contents, while

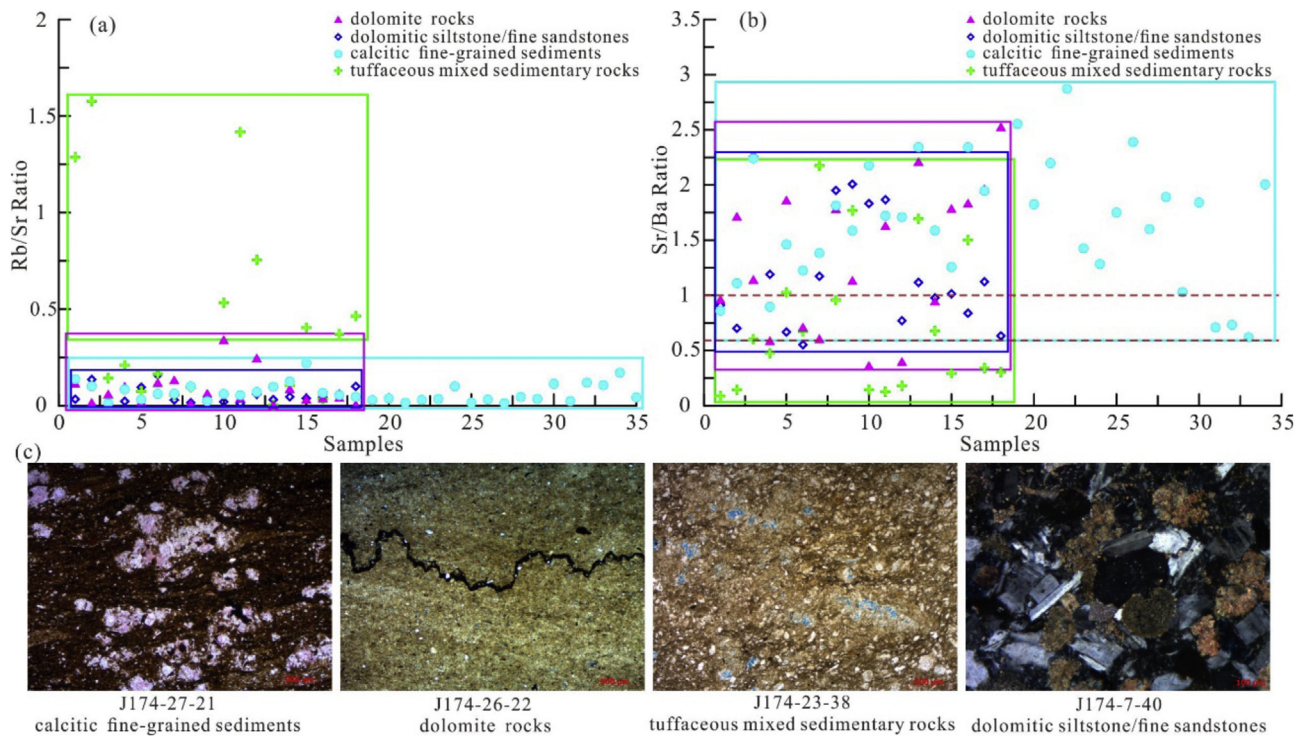


Fig. 15. Distribution of Rb/Sr ratio and Sr/Ba ratio values in different lithofacies. (a) High content of carbonate corresponds to low Rb/Sr ratio. (b) High content of carbonate corresponds to large Sr/Ba ratio. (c) Photomicrograph of the four rock types measured in (a) and (b).

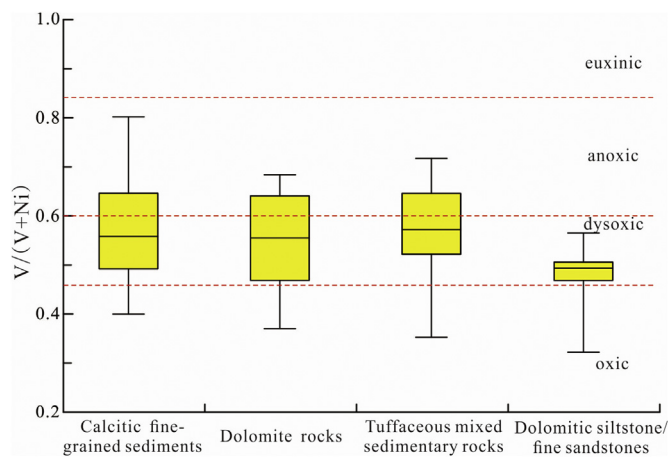


Fig. 16. V/(V+Ni) ratio values distribution of different rocks.

the silty dolomites show the opposite. Muddy tuffite, with much high Rb/Sr ratio values and Cr contents, moderate Ti/Al ratio and low Mn content, reflect a decreased paleo-salinity, a predominant more humid paleo-climate, decreased detrital clastics input and more reducing water conditions during depositional change from silty dolomite to muddy tuffite. In addition, the phosphorous contents and TOC were increased in the muddy tuffite rocks. The upper part (3142.4–3146 m) of the lower core interval comprises dolomite-rich rocks, with an upward change from micritic dolomites to silty dolomites, dolomitic siltstones and dolarenitic siltstones. The upper interval of the lower core show overall high Sr/Ba values and low Rb/Sr values, indicating deposition in brackish to salty water and an arid climate.

The complicated associations of lithofacies reflect frequent changes of sedimentary environment within the P₂l Formation. The lithofacies found in the P₂l₁² interval is mainly low-TOC dolomite-bearing

siltstones and high-TOC tuffaceous rocks, with less dolomite and limestone (Fig. 11). Geochemical element distribution indicates a low paleo-salinity, a weak reducing condition and a high terrigenous detrital input reflect under a relatively humid climate. The P₂l₁¹ interval is mainly composed of high-TOC fine-grained siltstones and mudstones, containing some micritic carbonate. Relatively humid climate began to prevail during the deposition of this interval, under deeper water, more reducing condition and low salinity, providing ideal conditions for pyrite precipitation and TOC accumulation. A subsequent shift towards more arid climate resulted in the fall of the lake level during the P₂l₂² interval, which was accompanied by higher salinity and more oxic conditions, as well as relatively limited terrigenous and pyroclastic input. Therefore, dolomite content increases during this interval resulting in lithofacies dominated by low-TOC silty grain dolostone/packstone, dolomiticrite and high-TOC muddy or tuffaceous dolomiticrite (Fig. 11). Higher up in the P₂l₂¹ interval, thin layers of mudstones with geochemical components indicate deepening water, reflecting a more humid climate, reducing conditions and lower paleo-salinity (Fig. 11).

Overall, the depositional environment of the P₂l Formation is characterized by relatively brackish, anoxia to reducing conditions under a relatively arid climatic setting. However, the depositional environment shows rapid and complex variations on small scale in the vertical profile.

5.3.2. Effect of sedimentary environmental setting on OM accumulation

The OM accumulation of the P₂l Formation is controlled by factors including terrestrial and tuffaceous inputs, redox conditions and primary productivity. Each factor may play a leading role in different intervals because of variations in the depositional environmental settings (Liang et al., 2018a, 2018b). The TOC content found in the lower section of the P₂l Formation (P₂l₁ interval) ranges widely from 0.34% to 15.51% (ave. = 3.11%). The cumulative thickness of strata containing TOC over 2% is about 91.75 m, corresponding to 58.81% of the entire P₂l₁ interval. During the deposition of the P₂l₁ interval, a relatively warm and humid climate enhanced algae growth (Cao et al., 2016). Deeper water, reducing conditions and volcanic ash input are favorable

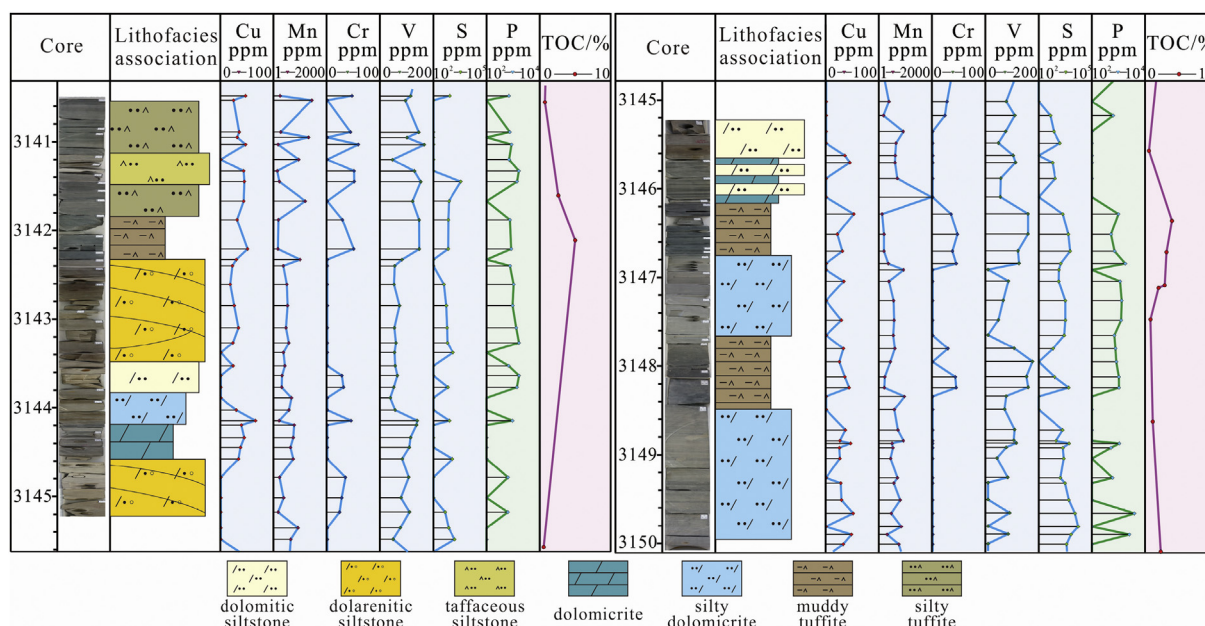


Fig. 17. Redox condition with element contents variations of the P_{2l} Formation in Well J-174, Jimusar Sag.

for algae accumulation, preservation and biodegradation, while relatively shallow water and terrestrial input have an inverse effect. The TOC of the upper section of the P_{2l} Formation (P_{2l_2} interval) ranges between 0.27% and 19.01% (ave. = 3.83%), and the cumulative thickness of strata with TOC over 2% is about 60.9 m, accounting for 60.9% of the entire P_{2l_2} interval. As a relatively arid climate prevailed during this period, the organic matter were derived mainly from higher plants, which has a limited impact on the oil-producing OM accumulation (Cao et al., 2016). Therefore volcanic ash input and resulted reducing saline condition are the main controlling factors for OM accumulation and preservation.

5.3.3. Implications for tight oil reservoir

Based on the analyses above, the TOC content and reservoir petrophysical properties of the P_{2l} Formation are influenced by sedimentary environmental conditions. Relatively deeper water, reducing conditions and input of volcanic ash are favorable for OM accumulation and preservation; at the same time, relatively coarse feldspar and debris grains, intraclast and volcanic input benefit the reservoir formation by dissolving. The rocks comprising more relatively coarse grains and less micritic dolomite tend to deposit under a high energy sedimentary setting, which are generally low paleo-salinity, weak reducing condition and high terrigenous detrital input, indicating a relatively humid climate. The unit contains interbedded high OM content rocks and high porosity reservoir will be the effective and favorable source-reservoir couplets for tight oil accumulation, as oil generated from the source rocks could directly charge into the adjacent reservoirs with primary or short secondary migration. Therefore, these stacked source and reservoir layers are good exploration targets for tight oil in the Lucaogou Formation.

6. Conclusions

The P_{2l} Formation in the Jimusar Sag is a typical example of fine-grained mixed sedimentary rock and tight oil reservoir in the Junggar Basin. Lithologies, provenances, depositional environmental settings and reservoir properties were detailed investigated. The results show that the fine-grained sedimentary rocks had three different sediment sources, external clastic input (terrigenous clastics), intrabasinal autochthonous to parautochthonous components (carbonates, siliceous skeletal debris and organic matter) and pyroclastic components, and four main lithofacies were recognized including siltstone/fine

sandstone, mudstone, dolomite and tuffite.

The carbonate rocks were generally deposited in warm and arid conditions, while the fine-grained clastic sediments were deposited under relatively humid conditions. The overall salinity of lake water was inferred to be brackish to salty, except for sections of the tuffaceous mixed sedimentary rocks and siltstones that were deposited in relatively fresh water. The muddy or silty tuffaceous mixed rocks and mudstones were deposited under more reducing conditions compared with the carbonate- and sandstones-rich rocks. Reducing conditions and volcanic ashes input played crucial roles in the formation of organic matter.

The main reservoir rock are tuffaceous siltstone, dolomitic siltstone, tuffaceous dolomiticrite, silty dolomiticrite and silty tuffite. Secondary dissolving pores are the most important reservoir space in the study area. Relatively coarse terrigenous grains and pyroclastics are benefit for formation of high porosity and permeability reservoirs. These rocks tend to deposit under a relatively humid climate with weak reducing condition and low paleo-salinity.

The lithology and OM accumulation of different intervals of the P_{2l} Formation show large differences as a result of interconnected factors including provenances, redox condition and climate during deposition. The depositional setting shows rapid and complex variations in the vertical profile, forming frequently alteration of reservoir and high-TOC source rocks and subsequently leading to the formation of potential tight oil plays.

Acknowledgements

This study is financially supported by the National Natural Science Foundation of China (Grant No.U1762217), the National Basic Research Program of China (Grant No.2014CB239002), and the National Science and Technology Special Grant, China (Grant No. 2016ZX05006-007). The Xinjiang Oilfield Company of PetroChina is thanked for providing all rock samples and some geological database. We also thank Jia Xiyu, Wan Min and Wang Xiatian from the Xinjiang Oilfield Company for their support of the work, and Hu Ruining and Yuan Erhui from China University of Petroleum for sample preparation. We are grateful to Helge Hellevang, Beyene Girma Haile and Clara Sena of University of Oslo for some insightful and stimulating discussion.

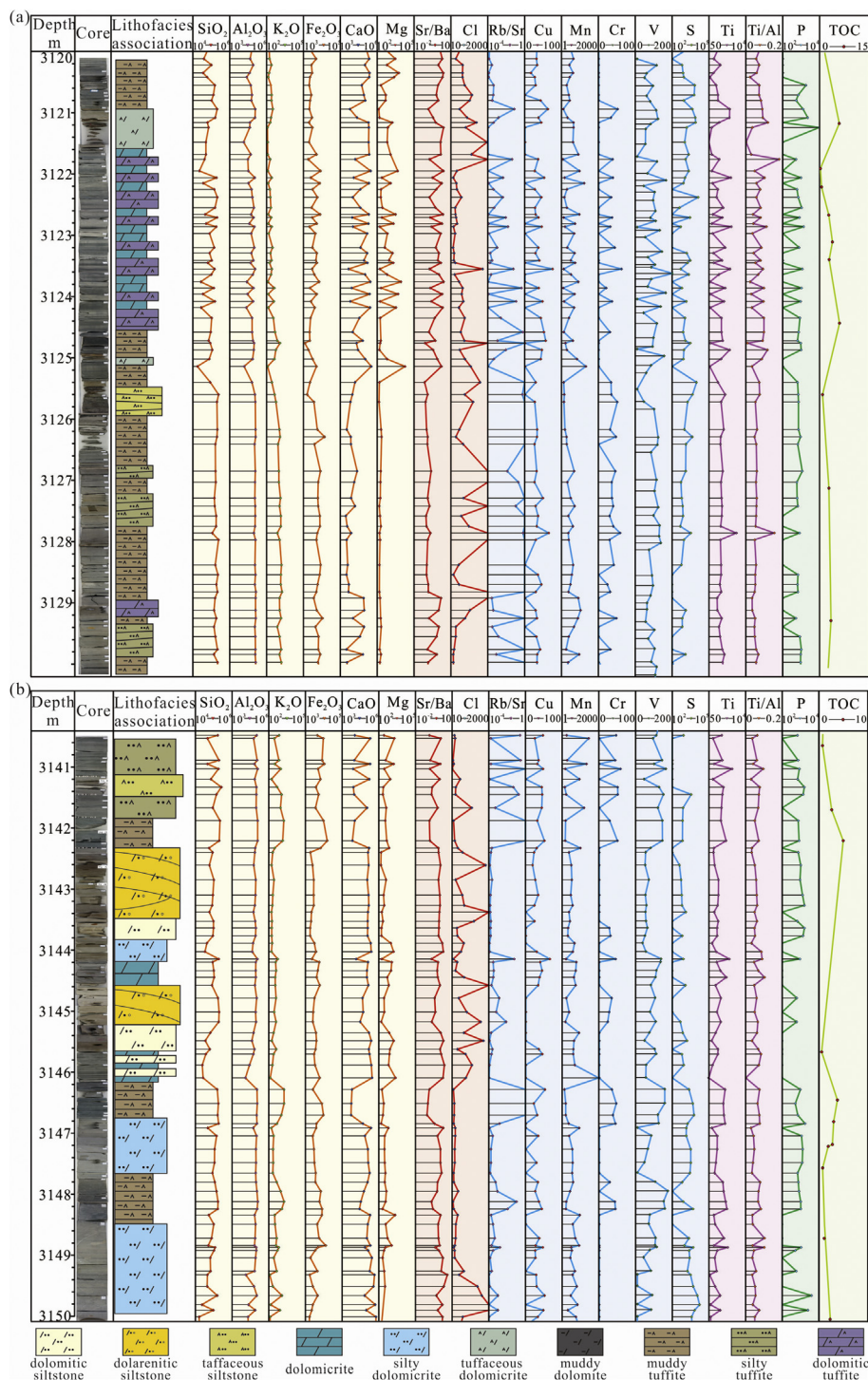


Fig. 18. Elements and geochemical parameter profile of (a) the 3120–3130 m interval in Well J-174 and (b) the 3141–3150 m interval in Well J-174, showing changing lithofacies of siltstone, tuffite and dolomite and their correlation with geochemical parameters.

Appendix A. Supplementary data

Supplementary data to this article can be found online at <https://doi.org/10.1016/j.marpetgeo.2018.10.039>.

References

Argast, S., Donnelly, T.W., 1987. The chemical discrimination of clastic sedimentary components. *J. Sediment. Res.* 57, 813–823.
 Bach, W., Irber, W., 1998. Rare earth element mobility in the oceanic lower sheeted dyke complex: evidence from geochemical data and leaching experiments. *Chem. Geol.*

151, 309–326.
 Bai, Y., Liu, Z., Sun, P., Liu, R., Hu, X., Zhao, H., Xu, Y., 2015. Rare earth and major element geochemistry of Eocene fine-grained sediments in oil shale and coal-bearing layers of the Meihe Basin, Northeast China. *J. Asian Earth Sci.* 97, 89–101.
 Berner, R.A., Raiswell, R., 1983. Burial of organic carbon and pyrite sulfur in sediments over Phanerozoic time: a new theory. *Geochem. Cosmochim. Acta* 47, 855–862.
 Bock, B., McLennan, S., Hanson, G., 1998. Geochemistry and provenance of the middle ordovician austin glen member (normanskill formation) and the taconian orogeny in new england. *Sedimentology* 45, 635–655.
 Cai, Z., Chen, F., Jia, Z., 2000. Types and tectonic evolution of Junggar Basin. *Earth Sci. Front.* 7, 431–440.
 Cao, Z., Liu, G., Kong, Y., Wang, C., Niu, Z., Zhang, J., Geng, C., Shan, X., Wei, Z., 2016. Lacustrine tight oil accumulation characteristics: permian Lucaogou Formation in

- Jimusaer sag, Junggar Basin. *Int. J. Coal Geol.* 153, 37–51.
- Chiarella, D., Longhitano, S.G., Tropeano, M., 2017. Types of mixing and heterogeneities in siliciclastic-carbonate sediments. *Mar. Petrol. Geol.* 88, 617–627.
- Drummond, C.N., Wilkinson, B.H., Lohmann, K.C., Smith, G.R., 1993. Effect of regional topography and hydrology on the lacustrine isotopic record of Miocene paleoclimate in the Rocky Mountains. *Palaeogeogr. Palaeoclimatol. Palaeoecol.* 101, 67–79.
- Fang, S., Song, Y., Xu, H., Fan, R., Liu, L., Xu, X., 2007. Relationship between tectonic evolution and petroleum system formation-taking the Jimusaer Sag of eastern Junggar Basin as an example. *Pet. Geol. Exp.* 29, 149–153.
- Harper, B.B., Puga-Bernabéu, Á., Droxler, A.W., Webster, J.M., Gischler, E., Tiwari, M., Lado-Insua, T., Thomas, A.L., Morgan, S., Jovane, L., 2015. Mixed Carbonate-siliciclastic sedimentation along the Great Barrier Reef upper slope: a challenge to the reciprocal sedimentation model. *J. Sediment. Res.* 85, 1019–1036.
- Haskin, M.A., Haskin, L.A., 1966. Rare earths in European shales: a redetermination. *Science* 154, 507–509.
- Hayashi, K.-I., Fujisawa, H., Holland, H.D., Ohmoto, H., 1997. Geochemistry of ~ 1.9 Ga sedimentary rocks from northeastern Labrador, Canada. *Geochem. Cosmochim. Acta* 61, 4115–4137.
- Jarvie, D.M., Hill, R.J., Ruble, T.E., Pollastro, R.M., 2007. Unconventional shale-gas systems: the Mississippian Barnett Shale of north-central Texas as one model for thermogenic shale-gas assessment. *AAPG Bull.* 91, 475–499.
- Jia, C., Zheng, M., Zhang, Y., 2012. Unconventional hydrocarbon resources in China and the prospect of exploration and development. *Petrol. Explor. Dev.* 39, 139–146.
- Jin, Z., Zhang, E., 2002. Paleoclimate implications of Rb/Sr ratios from lake sediments. *Sci. Technol. Eng.* 2, 20–22.
- Jones, B., Manning, D.A., 1994. Comparison of geochemical indices used for the interpretation of palaeoredox conditions in ancient mudstones. *Chem. Geol.* 111, 111–129.
- Kasanzu, C., Maboko, M.A., Many, S., 2008. Geochemistry of fine-grained clastic sedimentary rocks of the Neoproterozoic Ikorongo Group, NE Tanzania: implications for provenance and source rock weathering. *Precambrian Res.* 164, 201–213.
- Kuang, L., Hu, W., Wang, X., Wu, H., Wang, X., 2013. Research of the tight oil reservoir in the Lucaogou Formation in Jimusaer Sag: analysis of lithology and porosity characteristics. *Geol. J. China Univ.* 19, 529–535.
- Kuang, L., Yong, T., Dewen, L., Chang, Q., Ouyang, M., Lianhua, H., Deguang, L., 2012. Formation conditions and exploration potential of tight oil in the Permian saline lacustrine dolomitic rock, Junggar Basin, NW China. *Petrol. Explor. Dev.* 39, 700–711.
- Li, J., 2009. Study on the Oil Shale Geochemistry of Permian Lucaogou Formation in the Northern Bogda Mountain. Chinese University of Geosciences, Beijing (in Chinese).
- Liang, C., Jiang, Z., Cao, Y., Wu, J., Wang, Y., Hao, F., 2018a. Sedimentary characteristics and origin of lacustrine organic-rich shales in the salinized Eocene Dongying Depression. *GSA Bull.* 130, 154–174.
- Liang, C., Wu, J., Jiang, Z., Cao, Y., Song, G., 2018b. Sedimentary environmental controls on petrology and organic matter accumulation in the upper fourth member of the Shahejie Formation (Paleogene, Dongying depression, Bohai Bay Basin, China). *Int. J. Coal Geol.* 186, 1–13.
- Liang, Q., Jing, H., Gregoire, D.C., 2000. Determination of trace elements in granites by inductively coupled plasma mass spectrometry. *Talanta* 51, 507–513.
- Liu, C., Liu, K., Wang, X., Wu, L., Fan, Y., 2018. Chemostratigraphy and sedimentary facies analysis of the permian Lucaogou formation in the jimusaer sag, Junggar Basin, NW China: implications for tight oil exploration. *J. Asian Earth Sci.* <https://doi.org/10.1016/j.jseas.2018.04.001>.
- Luo, X., Wang, Z., Zhang, L., Yang, W., Liu, L., 2007. Overpressure generation and evolution in a compressional tectonic setting, the southern margin of Junggar Basin, northwestern China. *AAPG Bull.* 91, 1123–1139.
- Ma, J., Huang, Z., Zhong, D., Liang, S., Liang, H., Xue, D., Chen, X., Fan, Tang, 2016a. Formation and distribution of tuffaceous tight reservoirs in the permian tiaohu Formation in the malang sag, santanghu basin, NW China. *Petrol. Explor. Dev.* 43 (5), 714–722.
- Ma, K., Hou, J., Liu, Y., Shi, Y., Yan, L., Chen, F., 2017. The sedimentary model of saline lacustrine mixed sedimentation in Permian Lucaogou Formation, Jimusaer sag. *Acta Pet. Sin.* 38, 636–648.
- Ma, X., Li, M., Pang, X., Huang, Z., Jiang, Q., Li, Z., Cao, T., Li, Z., 2016b. Application of hand-held X-ray fluorescence spectrometry in the core analysis of Paleogene lacustrine shales in the Jiyang Depression. *Pet. Geol. Exp.* 38, 278–286.
- Maitre, L., 1989. A classification of igneous rocks and glossary of terms. In: Recommendations of the International Union of Geological Sciences Subcommittee on the Systematics of Igneous Rocks, vol 193.
- Mao, X., Li, J., Zhang, H., Wang, L., 2012. Study on the distribution and developmental environment of the Late Paleozoic volcanoes in Junggar Basin and its adjacent areas. *Acta Petrol. Sin.* 28, 2381–2391.
- McLennan, S.M., 1993. Weathering and global denudation. *J. Geol.* 101, 295–303.
- McNeill, D., Cunningham, K., Guertin, L., Anselmetti, F., 2004. Depositional themes of mixed carbonate-siliciclastics in the south Florida Neogene: application to ancient deposits. *AAPG Memoir* 80, 23–43.
- McNeill, D.F., Klaus, J.S., Budd, A.F., Lutz, B.P., Ishman, S.E., 2012. Late Neogene chronology and sequence stratigraphy of mixed carbonate-siliciclastic deposits of the Cibao Basin, Dominican Republic. *GSA Bull.* 124, 35–58.
- Meng, Q., Liu, Z., Hu, F., Sun, P., Liu, R., Zhou, R., Zhen, Z., 2013. Geochemical characteristics of Eocene oil shale and its geological significances in Huadian Basin. *J. Jilin Univ. (Earth Sci. Ed.)* 43, 390–399.
- Mongenot, T., Tribouillard, N.-P., Desprairies, A., Lallier-Vergès, E., Laggoun-Defarge, F., 1996. Trace elements as palaeoenvironmental markers in strongly mature hydrocarbon source rocks: the Cretaceous La Luna Formation of Venezuela. *Sediment. Geol.* 103, 23–37.
- Mount, J.F., 1984. Mixing of siliciclastic and carbonate sediments in shallow shelf environments. *Geology* 12, 432–435.
- Murray, R.W., Leinen, M., 1993. Chemical transport to the seafloor of the equatorial Pacific Ocean across a latitudinal transect at 135°W: tracking sedimentary major, trace, and rare earth element fluxes at the Equator and the Intertropical Convergence Zone. *Geochem. Cosmochim. Acta* 57, 4141–4163.
- Nesbitt, H., Young, G., 1982. Early Proterozoic climates and plate motions inferred from major element chemistry of lutites. *Nature* 299, 715.
- Peng, X., Wang, L., Jiang, L., 2012. Geochemical characteristics of the Lucaogou Formation oil shale in the southeastern margin of the Junggar Basin and its environmental implications. *Bull. China Soc. Mineral Petrol. Geochim.* 31, 121–157.
- Pollack, G.D., Krogstad, E.J., Bekker, A., 2009. U–Th–Pb–REE systematics of organic-rich shales from the ca. 2.15 Ga Sengoma Argillite Formation, Botswana: evidence for oxidative continental weathering during the Great Oxidation Event. *Chem. Geol.* 260, 172–185.
- Pommer, M., Milliken, K., 2015. Pore types and pore-size distributions across thermal maturity, Eagle Ford Formation, southern Texas. *AAPG (Am. Assoc. Pet. Geol.) Bull.* 99, 1713–1744.
- Rickwood, P.C., 1989. Boundary lines within petrologic diagrams which use oxides of major and minor elements. *Lithos* 22, 122–163.
- Riebe, C.S., Kirchner, J.W., Finkel, R.C., 2004. Erosional and climatic effects on long-term chemical weathering rates in granitic landscapes spanning diverse climate regimes. *Earth Planet Sci. Lett.* 224, 547–562.
- Robinson, P., 2003. XRF analysis of flux-fused discs. *Geoanalysis 2003*. In: The 5th International Conference on the Analysis of Geological and Environmental Materials, 2003.
- Rowe, H., Hughes, N., Robinson, K., 2012. The quantification and application of handheld energy-dispersive x-ray fluorescence (ED-XRF) in mudrock chemostratigraphy and geochemistry. *Chem. Geol.* 324–325, 122–131.
- Ryan, J., Shervais, J., Li, Y., Reagan, M., Li, H., Heaton, D., Godard, M., Kirchenbaur, M., Whattam, S., Pearce, J., 2017. Application of a handheld X-ray fluorescence spectrometer for real-time, high-density quantitative analysis of drilled igneous rocks and sediments during IODP expedition 352. *Chem. Geol.* 451, 55–66.
- Tanaka, K., Akagawa, F., Yamamoto, K., Tani, Y., Kawabe, I., Kawai, T., 2007. Rare earth element geochemistry of Lake Baikal sediment: its implication for geochemical response to climate change during the Last Glacial/Interglacial transition. *Quat. Sci. Rev.* 26, 1362–1368.
- Taylor, S., McLennan, S., 1985. *The Continental Crust: its Evolution and Composition*. Blackwell, London.
- Taylor, S.R., McLennan, S.M., 1995. The geochemical evolution of the continental crust. *Rev. Geophys.* 33, 241–265.
- Thranca, C., Talbot, M.R., 2006. High-frequency carbonate-siliciclastic cycles in the miocene of the lorca basin (western mediterranean, SE Spain). *Geol. Acta* 4, 343–354.
- Wang, L., Zhang, J., 1996. *Sedimentary Environment and Sedimentary Facies*. Petroleum Industry Press, Beijing.
- Wang, S., Song, S., He, D., 2013. The enrichment effect of organic materials by volcanic ash in sediments of the santanghu basin and the evolutionary pattern of tuffaceous source rocks. *Acta Pet. Sin.* 34, 1077–1087.
- Wesolowski, D.J., 1992. Aluminum speciation and equilibria in aqueous solution: I. The solubility of gibbsite in the system Na-K-Cl-OH-Al (OH) 4 from 0 to 100 °C. *Geochem. Cosmochim. Acta* 56, 1065–1091.
- Wu, H., Hu, W., Cao, J., Wang, X., Wang, X., Liao, Z., 2016. A unique lacustrine mixed dolomitic-clastic sequence for tight oil reservoir within the middle Permian Lucaogou Formation of the Junggar Basin, NW China: reservoir characteristics and origin. *Mar. Petrol. Geol.* 76, 115–132.
- Wu, H., Hu, W., Tang, Y., Cao, J., Wang, X., Wang, Y., Kang, X., 2017. The impact of organic fluids on the carbon isotopic compositions of carbonate-rich reservoirs: case study of the Lucaogou Formation in the Jimusaer Sag, Junggar Basin, NW China. *Mar. Petrol. Geol.* 85, 136–150.
- Xi, K., Cao, Y., Haile, B.G., Zhu, R., Jahren, J., Bjørlykke, K., Zhang, X., Hellevang, H., 2016. How does the pore-throat size control the reservoir quality and oiliness of tight sandstones? The case of the Lower Cretaceous Quantou Formation in the southern Songliao Basin, China. *Mar. Petrol. Geol.* 76, 1–15.
- Xi, K., Cao, Y., Zhu, R., Shao, Y., Xue, X., Wang, X., Gao, Y., Zhang, J., 2015. Rock types and characteristics of tight oil reservoir in Permian Lucaogou Formation, Jimusaer sag. *Acta Pet. Sin.* 36, 1495–1507.
- Xie, G., Yulin, S., Shugen, L., Weiduo, H., 2018. Trace and rare earth element (REE) characteristics of mudstones from eocene pinghu formation and oligocene huagang Formation in Xihu sag, east China sea basin: implications for provenance, depositional conditions and paleoclimate. *Mar. Petrol. Geol.* 92, 20–36.
- Xu, Q., Liu, B., Ma, Y., Song, X., Wang, Y., Chen, Z., 2017. Geological and geochemical characterization of lacustrine shale: a case study of the Jurassic Da'anzhai member shale in the central Sichuan Basin, southwest China. *J. Nat. Gas Sci. Eng.* 47, 124–139.
- Yang, Y., Qiu, L., Cao, Y., Chen, C., Lei, D., Wan, M., 2017. Reservoir quality and diagnosis of the permian Lucaogou formation tight carbonates in Jimusaer sag, Junggar Basin, west China. *J. Earth Sci.* 28 (6), 1032–1046.
- Yang, Z., Hou, L., Tao, S., Cui, J., Wu, S., Lin, S., Pan, S., 2015. Formation conditions and sweet spot evaluation of tight oil and shale oil. *Petrol. Explor. Dev.* 42, 555–565.
- Zhang, J., Jiang, Z., Liang, C., Wu, J., Xian, B., Li, Q., 2016. Lacustrine massive mudrock in the eocene Jiyang depression, Bohai Bay basin, China: nature, origin and significance. *Mar. Petrol. Geol.* 77, 1042–1055.
- Zhang, K., Jin, W., Lin, H., Dong, C., Wu, S., 2018a. Major and trace elemental compositions of the upper Carboniferous Batamayneishan mudrocks, Wulungu area, Junggar Basin, China: implications for controls on the formation of the organic-rich source rocks. *Mar. Petrol. Geol.* 91, 550–561.

- Zhang, S., Cao, Y., Zhu, R., Xi, K., Wang, J., Zhu, N., H, R., 2018b. Lithofacies classification of fine-grained mixed sedimentary rocks in permian Lucaogou formation, Jimusar sag, Junggar Basin. *Earth Sci. Front.* 25, 198–209. <http://doi.10.13745/j.esf.yx.2017-5-2>.
- Zhou, L., Friis, H., Poulsen, M.L.K., 2015. Geochemical evaluation of the late Paleocene and early Eocene shales in Siri Canyon, Danish-Norwegian basin. *Mar. Petrol. Geol.* 61, 111–122.
- Zou, C., Yang, Z., Tao, S., Li, W., Wu, S., Hou, L., Zhu, R., Yuan, X., Wang, L., Gao, X., 2012a. Nano-hydrocarbon and the accumulation in coexisting source and reservoir. *Petrol. Explor. Dev.* 39, 15–32.
- Zou, C., Zhu, R., Wu, S., Yang, Z., Tao, S., Yuan, X., Hou, L., Yang, H., Xu, C., Li, D., 2012b. Types, characteristics, genesis and prospects of conventional and unconventional hydrocarbon accumulations: taking tight oil and tight gas in China as an instance. *Acta Pet. Sin.* 33, 173–187.
- Zou, C., Zhu, R., Bai, B., Yang, Z., Hou, L., Zha, M., Fu, J., Shao, Y., Liu, K., Cao, H., 2015. Significance, geologic characteristics, resource potential and future challenges of tight oil and shale oil. *Acta Metall. Sin.* 34 (1), 3–17.